SHARING

SELF-ORGANIZED HETEROGENEOUS ADVANCED RADIO NETWORKS GENERATION

Deliverable D3.2

Multi-point cooperation schemes at the transmitter: innovative concepts and performance evaluation

Date of delivery	31/01/2015
Contractual date of delivery	31/01/2015
Project number	C2012/1-8
Editor(s)	Gregory Gougeon (SIR)
Author(s)	Gregory Gougeon (SIR), Mathieu Brau (SIR), Yves Lostanlen (SIR), Mari Kobayashi (SUP), Sheng Yang (SUP), Xinping Yi (EUR), Paul de Kerret (EUR), Sandeep Kottath (FT), Thierry Clessienne (FT), Nivine Abbas (FT), Nicolas Cassiau (CEA), Cécile Germond (TCS)
Dissemination level	PU
Workpackage	3
Version	v1.0
Total number of pages	56

Abstract:

In this document we assess innovative concepts at transmitter-side to suppress or avoid interference with CoMP and advanced MIMO schemes studied in task 3.1 of SHARING project. Channel State Information feedback designs are described to address the increasing backhaul constraint required for coordinating transmitters, or to maintain confidentiality between users during Multi-User transmissions. The impact on joint precoding of imperfect sharing of channel state information through the backhaul is also analytically studied. Several innovations are proposed to optimize fairness and network efficiency through advanced scheduling, Multi-User MIMO, mobility management or using linear dispersive codes at the transmitter. Finally, the impact of beamforming in a large-scale real environment is assessed.

Keywords: CoMP, coordinated scheduling, joint processing, MIMO, interference cancellation, beamforming.

Document Revision History

Version	Date	Author	Summary of main changes
0.1	03/11/2014	SIR	Creation of the document
0.2	10/12/2014	SIR	Integration of the contributions
0.3	09/01/2015	SIR	Document fix
1.0	04/02/2015	SIR	Final version

TABLE OF CONTENTS

EXECUTIVE SUMMARY

Deliverable D3.2 "Multi-point cooperation schemes at the transmitter: innovative concepts and performance evaluation" presents first performance evaluations of innovative concepts at transmitter-side to suppress or avoid interference with Coordinated Muti-Point (CoMP) and advanced MIMO schemes, resulting from the studies carried out within task 3.1 of SHARING project.

First studies explore the Channel State Information (CSI) limits for advanced MIMO schemes and CoMP.

Section 2.1 investigates the performance of a broadcast interference channel with secrecy constraint. It shows how the delayed CSI at the Transmitter (CSIT) can actually help in increasing the secrecy capacity in a proposed scheme inspired by the erasure broadcast channel secrecy.

Section 2.2 extends CSIT centralized configuration to an optimal distributed CSIT to minimize performance loss in a cooperative set of transmitters. A sufficient feedback rate is derived for the distributed CSIT configuration, ensuring that the rate loss compared to the transmission with perfect CSIT remains below a threshold value.

Section 2.3 evaluates the interest for a distance-based adaptive CSIT allocation in CoMP context. The proposed allocation appears as an alternative to base-stations clustering where the interference hard boundaries of the cluster are replaced by a smooth decrease of the cooperation strength.

Section 2.4 proposes an optimal user-centric clustering of base stations exploiting a broadcast feedback scheme. It enables exploiting additional out-of-cluster broadcast feedback, achieving a higher ergodic sum rate compared to a conventional scheme with similar number of feedback bits.

Then new advanced MIMO schemes and CoMP concepts are proposed.

Section 3.1 evaluates an opportunistic centralized scheduling approach where candidates to CoMP transmission are actually served using CoMP only if the resources are available, avoiding degrading other users (no CoMP) quality of service. This approach allows interesting gains at cell edge without impacting system capacity.

Section 3.2 assesses the performance of four interference aware receivers for Multi-User MIMO with LTE precoders. It is shown that implementing interference aware algorithms at the receiver is mandatory in Multi-User MIMO mode (LTE transmission mode 5). The "IA-ML" algorithm is shown to be the only one to cancel all interference in CoMP mode at the border of the cell.

Section 3.3 evaluates an opportunistic scheduling taking into account users mobility and channel fading, where users with best channel conditions are prioritized. It shows significant gains on average user throughput of both static and mobile users, as well as on mean cell-center and mean cell-edge throughput.

Section 3.4 assesses the performance of interference cancellation using linear dispersive codes at the transmitter and widely linear processing at the receiver. It improves the Bit Error Rate performance and enables to suppress internal interference with only one receiving antenna.

Finally, section 4 evaluates the impact of beamforming in a large-scale real environment.

The network performance is simulated thanks to a ray based propagation model and a realistic urban environment. The comparison with against without beamforming (LTE transmission mode 6) shows an increase of Signal to Noise plus Interference Ratio, as well as an improvement of mean user peak throughput.

Next deliverable D3.6 "Performance assessments of the most promising Multi-point transmission and reception techniques" will provide a more thorough full performance assessment of the most promising innovations described in this document.

1 INTRODUCTION

This deliverable presents first performance evaluations assessed through simulation of innovative concepts at transmitter-side to suppress or avoid interference with Coordinated Muti-Point (CoMP) and advanced MIMO schemes, in response to the challenges of Multi-point transmission identified in Task 3.1 and reported in deliverable D3.1.

With the aim of improving the Quality of Service (QoS) of users at cell edge, who suffer the most from inter-cell interference in LTE-A networks, the CoMP concept was first mentioned in [TR36.814] and introduced in [TR36.819]. In Task 3.1 we study transmitter-side solutions to suppress or avoid interference with CoMP and advanced MIMO schemes. Even though CoMP methods are extremely promising, this is a multi-faceted challenging problem. This can be seen from the fact that despite several years of intensive study under the auspices of 3GPP, it is still not clear which are the real gains to be expected from CoMP in cellular networks or which are the best signal processing and Radio Access Network (RAN) architectures. Through this task and a multi-angle attack we hope to shed some light on this area.

When using Joint Transmission (JT) technique, data is simultaneously transmited from multiple points (geographically separated or not) to a single User Equipment (UE) or multiple UEs in the same time-frequency resource, so as to improve the received signal quality and/or data throughput. The drawback is that the loss of resource in the set of cooperative eNodeBs (eNBs) causes a decrease in the global network spectral efficiency, thus the UEs to be served from multiple points result from a trade-off between fairness and network efficiency. In this document, several innovative concepts are evaluated to jointly optimize these two aspects, thanks to advanced scheduling, Multi-User MIMO or mobility management. One innovation evaluates a transmitter-side solution to suppress or avoid interference with advanced MIMO schemes, thanks to the use of linear dispersive spatial temporal codes at the transmitter combined to widely linear processing at the receiver. The advantage is that it can work in open loop and is thus not impacted by feedback issues.

Yet, another issue of CoMP and advanced MIMO schemes is the backhaul constraint. In the case of multi-antenna based interference reduction, we show that a key discriminating factor is the amount of feedback (Channel State Information at the Transmitter (CSIT)) allowed in the Uplink (UL). In Frequency Division Duplex (FDD), eNBs require the feedback from UEs to estimate the Downlink (DL) channel. The amount and the frequency of this feedback overload the UL, increase the UL interference and introduce delays in the channel estimation, with the number of cooperative points being a multiplicative factor. Hence feedback design studies are crucial and introduce another trade-off between feedback quantization and CoMP performance. Fundamental limits of advanced MIMO schemes with various CSI are studied, and several innovative concepts are evaluated to limit the feedback. One of these investigates the notion of wireless broadcast which, despite the fact that this is currently not LTE-compliant, exhibits interesting scalability benefits for dense small-cells networks.

Finally, a study illustrates the impact of beamforming in a large-scale real environment, using a ray-based propagation model combined to abstraction models for beamforming and interference.

The following of the document is organized as follows: section 2 focuses on the CSI limits of advanced MIMO schemes and CoMP, then four innovative concepts are described and evaluated in section 3. The impact of beamforming in a large-scale real environment is illustrated in section 4 and section 5 gives conclusions to this document.

2 CSI LIMITS OF ADVANCED MIMO SCHEMES AND COMP

2.1 Fundamental Limits of Advanced MIMO Schemes with Various CSI

We aim at investigating the performance of a multi-antenna broadcast channel with secrecy constraint such that each of messages must be conveyed to its intended receiver reliably while keeping it secret to unintended receivers. We address a practical scenario where the CSIT is completely outdated or delayed, i.e., independent of the current channel state. This setup, particularly relevant to fast fading channels where the channel training/feedback process incurs a delay larger than the coherence time, has paid significant attention recently [MAT12]. The main finding is that completely outdated CSIT enables to increase the Degree of Freedom (DoF) performance of multi-user networks by space and time interference alignment, characterizing the behavior of the capacity in the high Signal to Noise Ratio (SNR) regime [MAT12]. Similarly, our work [YKPS13] in the two-user multi-antenna broadcast channel showed that completely outdated CSIT is also useful to increase the secrecy capacity in the high SNR regime.

In this task, we wish to generalize the work [YKPS13] to a general case of K-user multi-antenna broadcast channel with confidential messages. As a performance measure, we consider the secrecy degrees of freedom (SDoF), the pre-log factor of the secrecy capacity that captures the behavior of the secrecy capacity in high SNR regime. Notice that the capacity of the multi-antenna broadcast channel remains open even without secrecy constraints. Our objective is to quantify the loss of DoF due to the additional secrecy constraints. Due to a space limitation, we illustrate only our achievable schemes and omit the converse results (and related proofs).

2.1.1 Revisiting two-user case

We first briefly recall the original Maddah-Ali and Tse (MAT) scheme without secrecy constraints and our proposed scheme: Yang, Kobayashi, Piantanida, and Shamai (YKPS) scheme with secrecy constraints for two-user MISO broadcast channel. The transmit antennas are two and each user has a single antenna. Without secrecy constraints, each user can achieve the DoF of 2/3 by the following three-slot MAT scheme:

$$\boldsymbol{x}_1 = \boldsymbol{v}_1, \quad \boldsymbol{x}_2 = \boldsymbol{v}_2, \qquad \boldsymbol{x}_3 = \begin{bmatrix} \mathbf{h}_2^{\mathrm{H}}[1]\boldsymbol{v}_1 + \mathbf{h}_1^{\mathrm{H}}[2]\boldsymbol{v}_2 \\ \mathbf{0} \end{bmatrix}, \tag{2.1}$$

Where $\boldsymbol{v}_1, \boldsymbol{v}_2$ denotes the confidential symbols for user 1, 2, respectively, $\mathbf{h}_k^{\mathrm{H}}[t]$ denotes the channel vector of user *k* at time *t*.

The first two time slots are to send two private symbols to each of users in TDMA. At the end of slot 2, each user has side information on the other user's symbols by overhearing. The role of slot 3 is to multicast a signal simultaneously useful for two users [MAT12]. This is done by sending a linear combination of the overheard signal at receiver 2 (in slot 1) and that at receiver 1 (in slot 2).

Now we consider the case of two confidential messages that must be secret to the unintended receiver. Under the secrecy constraints, SDoF of ½ can be ensured by the following four-slot scheme:

$$\begin{aligned} &\boldsymbol{x}_1 = \boldsymbol{u}, \boldsymbol{x}_2 = \boldsymbol{v}_1 + \begin{bmatrix} \mathbf{h}_1^{\mathrm{H}}[1]\boldsymbol{u} \\ \mathbf{0} \end{bmatrix}, \boldsymbol{x}_3 = \boldsymbol{v}_2 + \begin{bmatrix} \mathbf{h}_2^{\mathrm{H}}[1]\boldsymbol{u} \\ \mathbf{0} \end{bmatrix}, \\ &\boldsymbol{x}_4 = \begin{bmatrix} \mathbf{h}_2^{\mathrm{H}}[2]\boldsymbol{v}_1 + h_{21}[2]\mathbf{h}_1^{\mathrm{H}}[1]\boldsymbol{u} + \mathbf{h}_1^{\mathrm{H}}[3]\boldsymbol{v}_2 + h_{31}[3]\mathbf{h}_2^{\mathrm{H}}[1]\boldsymbol{u} \\ \mathbf{0} \end{bmatrix} \end{aligned} \tag{2.2}$$

where u denotes the artificial noise vector of dimension three.

Compared with MAT, the following remarks are in order:

1) the secrecy scheme consumes one time slot to generate the artificial noise;

2) thanks to delayed CSI the artificial noise received by each user will be **secretly** shared with the transmitter (up to the noise level);

3) the remaining three slots can be interpreted as secured MAT in which confidential symbols are protected by the artificial noise.

We can interpret the first time slot as the resource overhead necessary to ensure the additional secrecy constraints.

We also remark that for a special case of the MISO wiretap channel we just remove the third time slot by letting the confidential symbols v_2 for user 2 empty. In other words, the same amount of artificial noise is necessary even for sending one confidential message.

2.1.2 Connection with packet erasure channel with state-feedback

It is interesting to make a connection of YKPS scheme with the scheme proposed by Czap et al. for the erasure broadcast channel with state-feedback [CPDF14]. The channel output (state) of each receiver, either the channel input itself or an erasure, is fed back to the transmitter. This state-feedback enables the transmitter to perfectly know who has correctly received a packet and who has not. On the one hand, such knowledge can be used for ''opportunistic multicasting'' as for the MISO broadcast channel with delayed CSIT. Say user 1 (resp. 2) desires packet A (resp. B). If packet A is received by user 2 and packet B is received by user 1, the transmitter can send a packet corresponding to A X-OR B which is simultaneously useful for both, exactly in slot 3 of MAT scheme above. On the other hand, the state-feedback enables to create secret keys between the transmitter and a given user. If a packet is exclusively received by user 1, this packet can be used as a secret key. Motivated by these two observations, Czap et al. proposed the scheme consisting of two phases for a K-user erasure broadcast channel with state feedback ([CPDF14] and references therein). The first phase is to generate secret keys, while the second phase is to transmit encrypted messages via one-time pad. It should be noticed the same key can be reused until the unintended user receives it.

The first phase can be again interpreted as the resource overhead that is required to ensure the secrecy of each confidential message.

2.1.3 Three-antenna three-user case

Inspired by the scheme for the erasure broadcast channel with secrecy, we propose a two-phase scheme. The first phase is to create "analog'' secret keys via artificial noise transmission, while the second phase is to send confidential messages by a "secured'' version of MAT. The first phase of artificial noise transmission takes 4 slots; the second phase takes 11 slots. The second phase is divided in 6 slots for the order-1 symbol transmission, 3 slots for the order-2 symbol transmission, and 2 slots for the order-3 symbol transmission. We provide details of each step below as well as in Figure 1.

- Phase 1 (slot 1-4)

  The objective is to create analog secret keys, corresponding to the observation K_j of four dimensions at each receiver k =1, 2, 3. The transmitter sends artificial noise by using three antennas for 4 time slots. Thanks to delayed CSI, the transmitter knows three keys at the end of phase 1 (up to the background noise level).

- Phase 2
  - Phase 2.1 (slot 5-10)

    Send 6 confidential (order-1) symbols $\mathbf{v}_k$ embedded by the analog secret key K_k to each receiver by using three antennas. We let L_j denote two-dimensional overheard symbols. This phase creates 6 order-2 symbols, i.e. $\mathbf{V}_{12}$ for users 1 and 2, $\mathbf{V}_{13}$ for users 1 and 3, and $\mathbf{V}_{23}$ for users 2 and 3.

  - Phase 2.2 (slot 11-13)

Send 6 order-2 symbols $\mathbf{V}_{12}, \mathbf{V}_{13}, \mathbf{V}_{23}$ to each subset of two users by using two antennas as for the original MAT scheme. We let M_j denote a one-dimensional overheard symbol. This phase generates 2 order-3 symbols, V_{123}, U_{123}, two linearly independent combinations of M_3, M_5, M_7.

- Phase 2.3 (slot 14-15)

  Send two order-3 symbols by a single antenna as for the original MAT scheme.

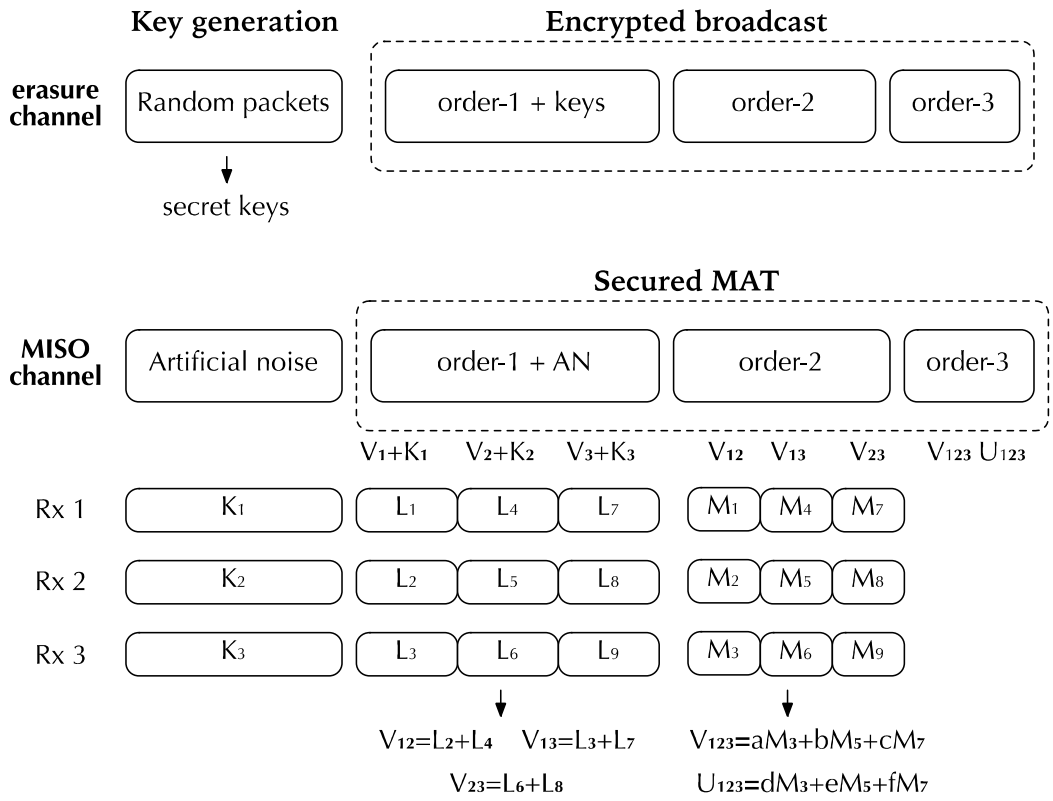

Figure 1: Three-antenna three-user secured broadcasting.

With this scheme, the transmitter can convey 6 confidential symbols to each user over 15 slots while keeping it secret to two others even if they collude. This results in SDoF of 2/5 each.

It is interesting to see that the proposed 15-slot scheme yields the following special cases of interest:

- MAT without secrecy constraints by removing phase 1 yields per-user DoF of 6/11;
- The two-user secrecy broadcasting by removing V3 (2 last slots in phase 2.1 and 1 lost in phase 2.3) yields per-user SDoF of 1/2;
- The wiretap channel by removing V2 and V3 (4 last slots in phase 2.1, 1 slot in phase 2.2, 1 slot in phase 2.3) yields SDoF of 2/3.

Each user performs decoding exactly as the same manner as the original MAT. It remains to show that the equivocation of each confidential message, i.e. that the confidential symbols of each user is not leaked to the other users even if they collude. For example, to show the equivocation of V1 to the collaborating receivers 2-3, note that V1 is observed through L2 and L3 to this virtual receiver. However the four-dimensional

subspace of L2 L3 is completely drowned in the artificial noise (or the secret key) K1. Therefore, it is impossible for the virtual receiver to recover V1 without knowing the secret key. The secret key K1 cannot be leaked to this virtual receiver either since the artificial noise spans in a 12-dimensional space and the observation spans in a reduced dimension of 8.

Finally, we can generalize this scheme to a general case of K-antenna K-user MISO broadcast channel.

The generalization is a work in progress and will be published in a conference paper shortly.

2.2 JP-CoMP with Limited Backhaul

2.2.1 Introduction

Determining the impact of imperfect CSI knowledge over the performance is critical in order to satisfy the required QoS and in terms of efficient system design. In the conventional *centralized* CSI configuration, a very important design guideline was provided in [JIN2006] where the scaling of the number of bits used for the CSI quantization to ensure a bounded rate loss in the broadcast channel when using Zero Forcing (ZF) was provided. Going further, a detailed analysis of the performance in the multi-user MIMO downlink was carried out in [CJK10] with very realistic feedback and training schemes.

In the distributed CSI configuration with each cooperating transmitter receiving its own multi-user channel estimate, the design guidelines from the literature are not longer valid and it remains to determine to which extend the results from the literature have to be modified when faced with distributed CSI.

In the following, we will first describe clearly the two CSI configurations, the *centralized* one, and the *distributed* one. We will then recall/adapt results from the literature for centralized CSI as they will be helpful for understanding and gain intuition when discussing the results obtained with distributed CSI.

2.2.2 System model

Transmission model

We study the transmission from *K* single-antenna TXs sharing the knowledge of the users' data symbols and using linear precoding to transmit to *K* single-antenna RXs which treat interference as noise. The channel from the *K* TXs to the *K* RXs is represented by the channel matrix $\mathbf{H}^{\mathrm{H}} \in \mathbb{C}^{K \times K}$ with its elements independent and identically distributed (i.i.d.) as $\mathcal{N}_{\mathbb{C}}(0,1)$ to model a uniform Rayleigh fading environment. We assume for simplicity that the pathloss is the same over all wireless links and the extension to channels with different pathloss is left for future works. The transmission is then described as:

$$\begin{bmatrix} y_1 \\ \vdots \\ y_K \end{bmatrix} = \mathbf{H}^{\mathrm{H}}\mathbf{x} + \boldsymbol{\eta} = \begin{bmatrix} \boldsymbol{h}_1^{\mathrm{H}}\mathbf{x} \\ \vdots \\ \boldsymbol{h}_K^{\mathrm{H}}\mathbf{x} \end{bmatrix} + \begin{bmatrix} \eta_1 \\ \vdots \\ \eta_K \end{bmatrix} \tag{2.3}$$

where y_i is the signal received at the *i*-th RX, $\boldsymbol{h}_i^{\mathrm{H}} \in \mathbb{C}^{1 \times K}$ the *i*-th channel to the *i*-th RX, and $\boldsymbol{\eta} \triangleq [\eta_1, \cdots, \eta_K]^{\mathrm{T}}$ the normalized Gaussian noise ($\mathcal{N}_{\mathbb{C}}(0,1)$). We denote the average per-TX transmit power by *P*. We also call *P* the "average SNR". The transmitted signal $\mathbf{x} = [\mathrm{x}_1, \cdots, \mathrm{x}_{\mathrm{K}}]^{\mathrm{T}}$ is obtained from the symbol vector $\boldsymbol{s} = [s_1, \cdots, s_K]^{\mathrm{T}}$ (i.i.d. $\mathcal{N}_{\mathbb{C}}(0,1)$) as

$$\mathbf{x} = \sqrt{P}\mathbf{U}\mathbf{s} = \sqrt{P}[\boldsymbol{u}_1 \quad \cdots \quad \boldsymbol{u}_K] \begin{bmatrix} s_1 \\ \vdots \\ s_K \end{bmatrix} \tag{2.4}$$

where $\mathbf{U} = [\mathbf{u}_1, \cdots, \mathbf{u}_K]$ is the unitary beamforming matrix and $\mathbf{u}_i$ is the beamforming vector used to transmit the data symbol s_i to RX *i*. Our focus being on the high-SNR interference-limited regime, we are interested in canceling out the interference. Hence,

we limit ourselves to studying ZF precoders. With perfect CSIT, the ZF unitary precoder denoted by $\mathbf{U}^{\star} = [\mathbf{u}_1^{\star}, \cdots, \mathbf{u}_K^{\star}]$ is written as

$$\mathbf{u}_i^{\star} \triangleq \left(\mathbf{I}_K - \mathbf{H}_i\left(\mathbf{H}_i^{\mathrm{H}}\mathbf{H}_i\right)^{-1}\mathbf{H}_i^{\mathrm{H}}\right)\boldsymbol{h}_i, \forall i \tag{2.5}$$

where

$$\mathbf{H}_i \triangleq [\boldsymbol{h}_1 \quad \ldots \quad \boldsymbol{h}_{i-1} \quad \boldsymbol{h}_{i+1} \quad \ldots \quad \boldsymbol{h}_K], \forall i. \tag{2.6}$$

The metric of interest in this work is the sum rate averaged over the channel realizations and, in case of imperfect CSIT, the quantization error of the channel estimate. With perfect CSI at the RX, the average rate of user i is written as

$$R_i \triangleq \mathrm{E}_{\mathcal{H},\mathcal{D}}\left[\log_2\left(1 + \frac{P\left|\boldsymbol{h}_i^{\mathrm{H}}\mathbf{u}_i\right|^2}{1 + \sum_{j\neq i} P\left|\boldsymbol{h}_i^{\mathrm{H}}\mathbf{u}_j\right|^2}\right)\right]. \tag{2.7}$$

CSI Configuration

- Broadcast Channel (BC) with centralized CSIT:

In the conventional centralized CSIT configuration, all the TX antennas are colocated and share *perfectly* a single multi-user imperfect channel estimate $\widehat{\mathbf{H}} = [\hat{\mathbf{h}}_1, \cdots, \hat{\mathbf{h}}_K]^{\mathrm{H}}$.The imperfect channel estimate is then modeled as

$$\widehat{\boldsymbol{h}}_i = \sqrt{1-\sigma^2}\boldsymbol{h}_i + \sigma\boldsymbol{\delta}_i \tag{2.8}$$

with σ being the variance of the quantization/feedback error.

- Broadcast Channel (BC) with distributed CSIT:

In the BC with distributed CSIT, TX j has its own estimate of the global multi-user channel denoted by $\widehat{\mathbf{H}}^{(j)} = [\hat{\mathbf{h}}_1^{(\mathrm{j})}, \cdots, \hat{\mathbf{h}}_K^{(\mathrm{j})}]^{\mathrm{H}}$. We then also model this quantized estimate as

$$\hat{\mathbf{h}}_i^{(\mathrm{j})} = \sqrt{1-\sigma^2}\mathbf{h}_i + \sigma\boldsymbol{\delta}_i^{(\mathrm{j})}. \tag{2.9}$$

A practical scenario where the CSIT is distributed arises when the CSI is broadcast from the RXs to the noncolocated TXs in an analog manner (analog feedback). In fact, the digital quantization model used in this work is solely a model to represent the error in the CSIT due to the limited feeeback and the results can be directly extended to the case of analog feedback. In this case, the number of feedback bits can be related to the average transmit power (or bandwidth) on the feedback channel.
Note that the channel estimate at every TX could potentially have a different accuracy but we study in this work the configuration where the estimates at all the TXs are of the same quality, i.e., they have the same statistical properties.

2.2.3 Preliminaries: Feedback Analysis with centralized CSI

We study in this section the feedback design in the conventional K-user MISO BC with centralized CSIT. The scaling of the number of feedback bits in terms of the average transmit SNR *P* is a well known result (See [JIN06, CJK10] among others). Yet, we consider in this work a slightly different power normalization which is more adapted to the model of distributed CSIT, such that the results from the literature cannot be directly applied. Furthermore, we provide additional insights by studying the interference term $|\mathbf{h}_i^{\mathrm{H}}\mathbf{u}_k|^2, i \neq k$ which represents the interference at RX *i* resulting from the transmission to RX k.

Proposition *(Interference scaling for centralized CSI):* In the BC with centralized CSIT and $\sigma^2 = 2^{-B}$, with B being the number of bits used to quantize each channel

element, there is a subspace $\mathcal{A}_\sigma$ of probability 1 such that

$$\mathrm{E}_{\mathcal{A}_\sigma}\left[|\mathbf{h}_i^{\mathrm{H}}\mathbf{u}_j^{\mathrm{CCSI}}|^2\right] \leq \sigma^2. \tag{2.10}$$

The variance of the interference term $|\mathbf{h}_i^{\mathrm{H}}\mathbf{u}_k|^2, i \neq k$ is a very important figure of merit since it represents the power of the leaked interference after ZF. Building upon this first result, the following sufficient CSIT allocation can be obtained.

Theorem *(CSI scaling for centralized CSIT)*: At high SNR in the BC with centralized CSIT and $\sigma^2 = 2^{-B}$, the rate loss is upper bounded by $\log(1+b)+o(1)$ bits if $\mathrm{B} = \mathrm{B}^{\mathrm{CCSI}}$ given by

$$\mathrm{B}^{\mathrm{CCSI}} \triangleq K\log_2\big((K-1)P\big) - K\log_2(b). \tag{2.11}$$

It is intuitive that the distributedness of the CSIT leads to an increased amount of leaked interference since the precoding coefficients are less coordinated. However, this degradation has not yet been quantified and the feedback requirements with distributed CSIT are unknown.

2.2.4 Feedback Analysis with Distributed CSI

The main goal of this section is to obtain a counterpart for the feedback design guideline provided for the case of centralized CSIT when the transmitter is faced with distributed CSIT. Due to the distributed precoding, the distribution of the leaked interference $|\mathbf{h}_i^{\mathrm{H}}\mathbf{u}_k|^2, i \neq k$ is more complicated and cannot be easily obtained. To study this term, we start by evaluating the difference $\|\mathbf{u}_k^* - \mathbf{u}_k^{(j)}\|$.

Proposition *(MSE scaling):* In the BC with distributed CSIT and $\sigma^2 = 2^{-B}$ it holds with probability one that

$$\mathbf{u}_k^{(\mathrm{j})} = \mathbf{u}_k^\star + \mathbf{a}_k^{(\mathrm{j})} + o(\sigma) \tag{2.12}$$

with

$$\mathrm{E}\left[\left\|\mathbf{a}_k^{(\mathrm{j})}\right\|^2\right] = (2K-1)\sigma^2. \tag{2.13}$$

As the precoding at each of the TX is the same as in the case of centralized CSIT, this proposition is also valid for the precoder $\mathbf{u}_k^{\mathrm{CCSI}}$ obtained using centralized CSI.We can now use this proposition to state our main result.

Theorem *(CSI Scaling with distributed CSIT):* At high SNR in the BC with distributed CSIT, the rate loss is upper-bounded by $\log(1+b)+o(1)$ bits if $\mathrm{b} > 2 + 2\log(K)$ and $\mathrm{B} = \mathrm{B}^{\mathrm{DCSI}}$ being given by:

$$\mathrm{B}^{\mathrm{DCSI}} \triangleq K\log_2\big((2K-1)(K-1)P\big) - K\log_2\left(\frac{b-2-2\log(K)}{3+2\log(K)}\right). \tag{2.14}$$

Considering *K* large, it follows that the feedback rate should be roughly $\mathrm{K}\log_2(\mathrm{K})$ larger when the CSIT is distributed compared to the centralized case so as to ensure that the rate loss is below the same threshold value. The second term in the right-hand side is the reason behind the condition on *b* in the theorem. Yet, it is believed to be an artifact from the proof due to technical difficulties in the calculation, and that both the restriction on the values taken by *b* and this additional term could be removed at the cost of the addition of a (small) constant in the expression$\mathrm{B}^{\mathrm{DCSI}}$.

2.2.5 Simulation Results

We will verify by simulations the analytical results using 100 000 Monte-Carlo realizations of the channel and the quantization errors in the case of a K users Rayleigh fading channel with all the channel links having a unit variance. First, we show in Figure 2 the average value of the MSE $\|\mathbf{u}_k^* - \mathbf{u}_k^{(j)}\|$as a function of the variance of the quantization error

σ^2 when $K = 5$. Since we are interested in the high precision quantization, we consider small values of σ^2. The simulations can be seen to overlap exactly with the theoretical results from the proposition as the slope of both curves is $(2K - 1) = 9$.

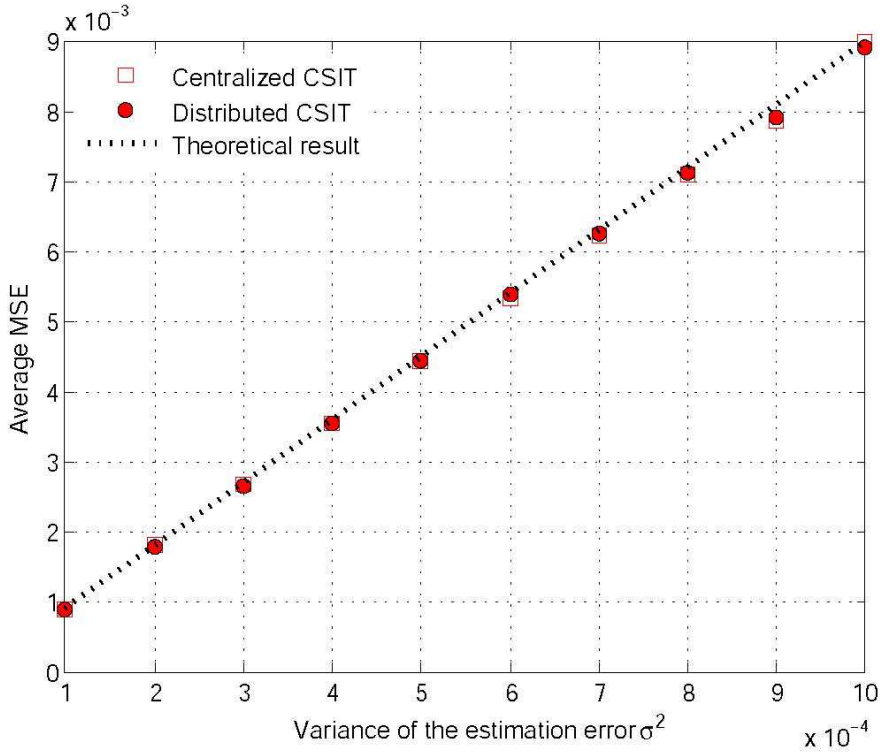

Figure 2: Average value of the MSE $\|\mathbf{u}_k^* - \mathbf{u}_k^{(j)}\|$ as a function of σ^2.

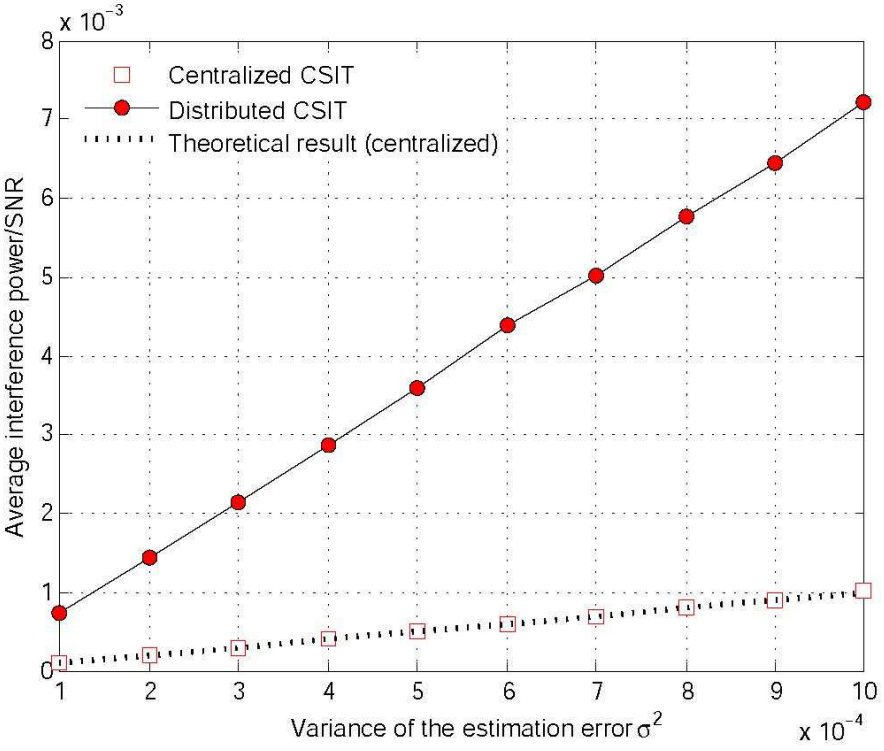

Figure 3: Average value of the leaked interference $\mathrm{E}\left[|\mathbf{h}_i^{\mathrm{H}}\mathbf{u}_j^{\mathrm{CCSI}}|^2\right]$ (resp. $\left[|\mathbf{h}_i^{\mathrm{H}}\mathbf{u}_j^{\mathrm{DCSI}}|^2\right]$) after normalization by the average SNR as a function of σ^2.

We show then in Figure 3 the average interference power after normalization by the average SNR *P*. We see in the simulations that the average leaked interference seems to be exactly equal to σ^2 in the case of centralized CSIT. This is in fact a predictable result. Indeed, using a different modelization of the quantization error, where we have this time $\mathbf{h}_i = \hat{\mathbf{h}}_i + \sigma\boldsymbol{\delta}_i$ with the quantization error $\boldsymbol{\delta}_i$ independent of the estimate $\hat{\mathbf{h}}_i$, it is easily shown that the expectation of the inner product is exactly equal to σ^2.

Finally, the average rate per user in the BC with distributed CSIT is shown in terms of the average SNR in Figure 4 for $K = 15$. We show the average rate achieved when perfect CSIT is available at the TXs and we compare it to the rate achieved with limited feedback using different number of feedback bits. We consider a digital feedback with B^{DCSI} for $\mathrm{b} = 5 + 3\log(\mathrm{K})$ and with B^{CCSI} given in the theorem for the same value of b. Using B^{DCSI} leads to a rate loss smaller than 1 bit while the upper bound for the rate loss per user was log2(1 + b)=4.0732 bits. This is in agreement with our conjecture that the second term of the feedback rate given in the Theorem could be replaced by a (small) constant. Indeed, according to this conjecture, using $b = 5 + 4\log(K)$ in the feedback rate of the theorem corresponds approximately to using b=1 in our conjectured feedback rate which gives a rate loss of 1 bit. Using B^{CCSI} leads to a very significant rate loss as the CSI inconsistencies between the TXs are not taken into account.

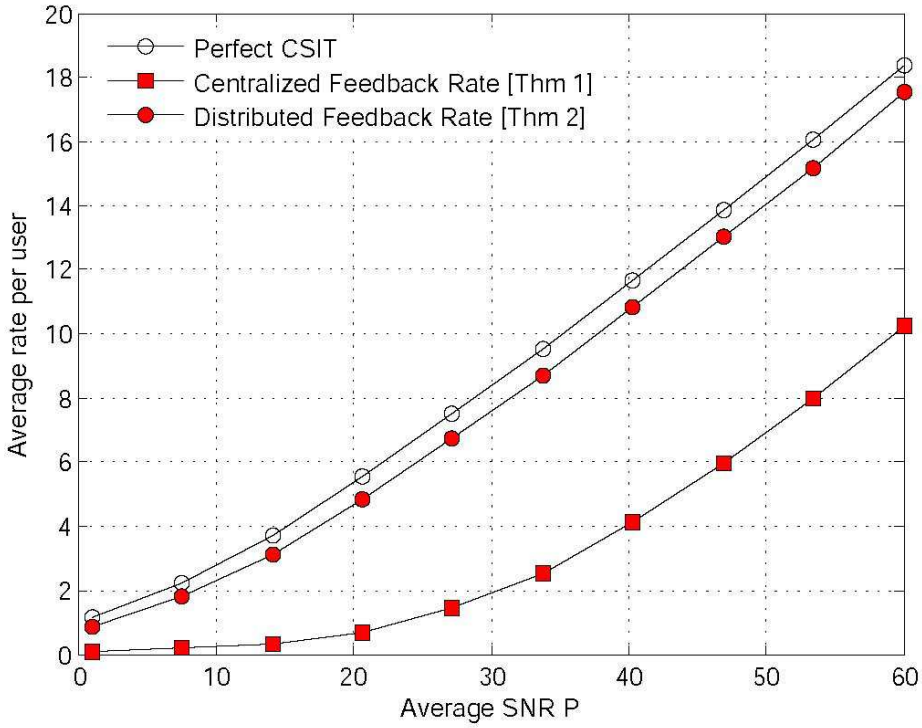

Figure 4: Average rate per –user as a function of the average SNR P for $K = 15$.

2.2.6 Discussion of the Results

Considering a distributed CSIT configuration where every TX has its own channel estimate and cooperates with the other TXs without any additional exchange of information, we have derived a sufficient feedback rate which ensures that the rate loss compared to the transmission with perfect CSIT remains below a threshold value. Interestingly, the expression obtained in the provided theorem can be seen to increase more quickly with the number of users K than its counterpart in the BC with "centralized" CSIT. Hence, the CSI discrepancies resulting from the distributedness of the CSIT can lead to important performance degradations, if not taken into account in the feedback design. An upper-bound for the rate loss for a given amount of feedback has been derived and the derivation of a lower-bound is the focus of undergoing research.

However, the statistical distribution of the interference with distributed CSIT makes this problem relatively intricate. Furthermore, the extension of the analysis to scenarios with different pathloss between every TX and every RX represents a challenging and interesting research problem.

2.3 Spatial CSIT Allocation for JP-CoMP Schemes

2.3.1 Introduction

Joint transmission from distributed TXs is the most powerful cooperation method and allows to completely suppress interference and serve jointly all the users. However, it imposes strong requirements over the network architecture in order to allow for this tight coordination between the distributed TXs. One of the biggest challenges comes from the need to obtain **global** CSI at each TX. Indeed, the local CSI has then to be exchange to all the cooperating nodes or to be transferred to a central node where the computation of the precoder is done. In both cases, this approach does not scale well with the number of cooperating TXs and becomes quickly unrealistic.

However, the joint transmission schemes from the literature consider that the joint precoding is done in a centralized manner, or equivalently distributed at the TXs but with each TX having access to the same CSI. In the following, we challenge this assumption and consider a transmission scenario where each TX receives its own version of the CSI. Indeed, it is very intuitive that in a very large network, each TX should have a more accurate knowledge of its neighborhood than of the channel relative to distant TXs or RXs. Our main goal in this work is to provide quantitative results building upon this intuitive result. In particular, we will show that it is possible to achieve **global coordination** with only **local CSI exchange.**

2.3.2 System Model

Transmission model

We consider a network MIMO setting in which K non-colocated TXs transmit jointly via linear precoding to K RXs equipped with a single antenna and applying single user decoding. Each TX initially has the knowledge of the K data symbols to transmit to the K RXs (owing to TX cooperation friendly routing protocol for user-plane data). Note that this assumption will be discussed later in this work.

The transmission is then described as

$$\begin{bmatrix} y_1 \\ \vdots \\ y_K \end{bmatrix} = \mathbf{H}^{\mathrm{H}}\mathbf{x} + \boldsymbol{\eta} = \begin{bmatrix} \boldsymbol{h}_1^{\mathrm{H}}\mathbf{x} \\ \vdots \\ \boldsymbol{h}_K^{\mathrm{H}}\mathbf{x} \end{bmatrix} + \begin{bmatrix} \eta_1 \\ \vdots \\ \eta_K \end{bmatrix} \tag{2.15}$$

where $\boldsymbol{y} = [y_1, \cdots, y_K]^{\mathrm{T}}$ contains the received signals at the K RXs, $\mathbf{h}_i^{\mathbf{H}}$is the channel to the *i*-th RX, $\boldsymbol{\eta} = [\eta_1, \cdots, \eta_K]^{\mathrm{T}}$ is the i.i.d. unit variance Gaussian normalized noise at the RXs, and $\boldsymbol{x} = [x_1, \cdots, x_K]^{\mathrm{T}}$epresents the transmit signals at the K TXs.

We also define the multi-user channel $\mathbf{H}^{\mathrm{H}} \triangleq [\mathbf{h}_1, \cdots, \mathbf{h}_K]^{\mathrm{H}}$. The channel coefficient $H_{k,i}$ designates the fading coefficient between TX *i* and RX *k*. We consider a Rayleigh fast fading channel such that $H_{k,i} = \sigma_{k,i}^2 \widetilde{H}_{k,i}$ where $\widetilde{H}_{k,i}$ is a standard Gaussian random variable distributed as $\mathcal{N}_{\mathbb{C}}(0,1)$. The parameter $\sigma_{k,i}^2$ is the variance of the channel coefficient and hence represents the long term attenuation or the geometry (topology) of the network. We consider in the following for the sake of clarity that $\forall i, \sigma_{i,i}^2 = 1$.

The transmit signal $\mathbf{x}$ is obtained from the user's data symbols $\boldsymbol{s} = [s_1, \cdots, s_K]^{\mathrm{T}}$

(i.i.d. $\mathcal{N}_{\mathbb{C}}(0,1)$) as

$$\mathbf{x} = [\boldsymbol{t}_1 \quad \dots \quad \boldsymbol{t}_K] \begin{bmatrix} s_1 \\ \vdots \\ s_K \end{bmatrix}. \tag{2.16}$$

Hence, the vector $\boldsymbol{t}_i$ represents the beamforming vector used to transmit s_i to RX i and we define as $\mathbf{T} = [\mathbf{t}_1, \cdots, \mathbf{t}_K]$ the multi-user joint precoder. We consider a sum power constraint and an equal power allocation to the users, both for clarity and because it does not impact the conventional DoF. Note that because of the normalization of the noise and of the direct channels, P denotes also the average per-stream SNR. The ergodic rate of user i is written as

$$R_i \triangleq \mathrm{E}\left[\log_2\left(1 + \frac{|\mathbf{h}_i^{\mathrm{H}}\mathbf{t}_i|^2,}{1 + \sum_{i \neq k} |\mathbf{h}_i^{\mathrm{H}}\mathbf{t}_k|^2}\right)\right]. \tag{2.17}$$

The conventional DoF at RX i is defined as commonly used in the literature as

$$\mathrm{DoF}_i \triangleq \lim_{\mathrm{P}\to\infty} \frac{R_i}{\log_2(\mathrm{P})}. \tag{2.18}$$

The DoF achieved at RX i is then the prelog factor with which the ergodic rate increases as a function of the SNR, in the large SNR regime. Note that the channel elements are all non-zero with probability one. Considering only these channel realizations does not reduce the DoF achieved but has for consequence that all the expectations can be shown to exist. For the sake of clarity, we consider then only these channel realizations in the following.

Generalized DoF Analysis

However, we aim in this work at studying the effect of the network topology in the high SNR performance. In the conventional DoF analysis, any finite pathloss difference is neglected. This leads in some cases to a significant gap between the predicted and the true performance at finite SNR. As a consequence, we use the notion of generalized DoF [ETW08] as a way to obtain a more accurate modeling of the performance. In the generalized DoF approach, the attenuation of the interference is represented as an exponential function of the transmit power so as to preserve the impact of the network geometry in the high SNR analysis. Hence, the generalized DoF at RX i is defined as

$$\mathrm{DoF}_i\left(\{\mathbf{B}^j\}_{j=1}^K, \boldsymbol{\Gamma}\right) \triangleq \lim_{\mathrm{P}\to\infty} \frac{R_i}{\log_2(\mathrm{P})} \text{ subject to } \sigma_{k,i}^2 = \mathrm{P}^{-\{\Gamma\}_{k,i}}, \forall k, i \tag{2.19}$$

where the CSIT allocation $\{\mathbf{B}^j\}_{j=1}^K$and the precoding used will be described in the following and the matrix $\boldsymbol{\Gamma} \in [0,\infty]^{K\times K}$ is called the "*interference level matrix*" and is given as a function of the parameters of the practical network being studied. Its (k,i)-th element is then denoted by $\Gamma_{k,i}$. More specifically, our goal is to model the transmission in a realistic network (Hence with finite pathloss and finite transmit SNR) in the most accurate possible way, and the interference level matrix makes the link between the practical network and the model obtained. Denoting by P_0 the finite power used in practice and by $\sigma_{k,i,0}$ the variance of the channel coefficient between TX i and RX k in the practical setting, the interference level matrix is then defined as

$$\Gamma_{k,i} \triangleq -\frac{\log_2\left(\sigma_{k,i,0}^2\right)}{\log_2(\mathrm{P}_0)}, \forall k, i. \tag{2.20}$$

Note that we assume that all the diagonal coefficients of the interference-level matrix are equal to zero, i.e., $\Gamma_{i,i} = 0$.

As already discussed in the introduction, the goal of the generalized DoF is not to model an unrealistic channel where the pathloss increases with the SNR, in the same way that a DoF analysis does not really apply for transmission with infinite amount of power. It

consists simply, starting from a practical setting, in letting both the SNR and the pathloss increase at the same time (instead of letting simply the SNR increase for the conventional DoF analysis). This ensures that the differences of power between the wireless links do not become negligible when considering the high SNR regime and hence allows us to take into account the geometry of the network.

Remark: When P_0 – the transmit power used in the practical setting– tends to infinity, the prelog factor converges to the (conventional) DoF. The prelog factor converges to the generalized DoF in a different limiting regime where both the pathloss and the SNR increase at the same time. This could for example be the case if the transmit power is made dependent of the distance between the TXs and the RXs. Both approaches however can be used to approximate the performance in practical settings at finite (high) SNR. When there are significant pathloss differences, the generalized DoF will be more accurate.

Example: Let us consider as toy example a Gaussian interference channel with two TX/RX pairs and every node having a single-antenna. They interfere to each other via a channel of variance $\sigma^2 \in (0,1)$ while the direct links have unit variance. The DoF is well known to be equal to 0.5 independently of the value of σ^2 However, if the TXs interfere with very low power, e.g., $\sigma^2 = 10^{-12}$, then the interference will be negligible for any realistic range of power used for the transmission. Considering a transmission at SNR $P_0 = 30\ \mathrm{dB}$, the interfering coefficient as defined in [ETW08] would be

$$\alpha = \max\left(\frac{\log_2(P_0\sigma^2)}{\log_2(P_0)} \quad , \quad 0\right) = 0. \tag{2.21}$$

The generalized DoF would then be equal to$1-\alpha = 1$. Hence, the generalized DoF analysis models more accurately the transmission in that setting.

Distributed CSI at the TXs

The joint precoder is implemented distributively at the TXs with each TX relying solely on its own estimate of the channel matrix in order to compute its transmit coefficient, without any exchange of information with the other TXs [KG12,ZG10]. To model the imperfect CSI at the TX (CSIT), the channel estimate at each TX is assumed to be obtained from a limited rate digital feedback scheme. Consequently, we introduce the following definitions.

Definition *(Distributed Finite-Rate CSIT):* We represent a CSIT allocation by the collection of matrices $\{\mathbf{B}^{(j)}\}_{j=1}^{K}$where $\mathbf{B}^{(j)} \in \mathbb{C}^{K\times K}$ denotes the CSIT allocation at TX *j*. Hence, TX *j*receives the multi-user channel estimate $\mathbf{H}^{(j)}$ defined from

$$\widetilde{H}_{k,i}^{(j)} = \sigma_{k,i} H_{k,i}^{(j)} + \sigma_{k,i}\sqrt{2^{-B_{k,i}^{(j)}}}\,\Delta\widetilde{H}_{k,i}^{(j)} \tag{2.22}$$

where $\Delta\widetilde{H}_{k,i}^{(j)} \sim \mathcal{N}_{\mathbb{C}}(0,1)$and the $\Delta\widetilde{H}_{k,i}^{(j)}$are mutually independent and independent of the channel.

Remark: The reasons for modeling the imperfect CSIT under the previous equation are as follows. First, it is well known from rate-distortion theory that the minimal distortion when quantizing a standard Gaussian source using *B* bits is equal to 2^{-B} [CT06, Theorem 13.3.3] while this distortion value is also achieved up to a multiplicative constant using for example the Lloyd algorithm or even scalar quantization. Thus, the decay in 2^{-B} as the number of quantization bits increases represents a reasonable model.

Furthermore, only the asymptotic behavior exponentially in the SNR is of interest in this work such that the distribution of the CSIT error does not matter. We have chosen a Gaussian model for simplicity but other distributions fulfilling some mild regularity constraints could be chosen.

It is a well known result that the number of CSI feedback bits should scale with the SNR in order to achieve a positive DoF in MISO BCs [JIN06, CJK10]. Hence, the prelog factor represents an appropriate measure at high SNR of the amount of CSIT required. Thus, we define the size of a CSIT allocation as follows.

Definition*(Size of a CSIT allocation)*: The size s(•) of a CSIT allocation $\mathbf{B}^{(j)}$at TX j is defined as

$$s\left(\mathbf{B}^{(j)}\right) \triangleq \lim_{\mathrm{P}\to\infty} \frac{\sum_{i,k} B_{k,i}^{(j)}}{\log_2(\mathrm{P})} \tag{2.23}$$

such that the total size of a CSIT allocation $s\left(\{\mathbf{B}^{(j)}\}_{j=1}^{K}\right)$is

$$s\left(\left\{\mathbf{B}^{(j)}\right\}_{j=1}^{K}\right) \triangleq \sum_{j=1}^{K} s\left(\mathbf{B}^{(j)}\right) = \lim_{\mathrm{P}\to\infty} \frac{\sum_{i,j,k} B_{k,i}^{(j)}}{\log_2(\mathrm{P})}. \tag{2.24}$$

Remark: We consider here a digital quantization of the channel vectors but the results can be easily translated to a setting where analog feedback is used. Indeed, digital quantization is simply used as a way to quantify the variance of the CSIT errors. Furthermore, only CSI requirements at the TXs are investigated, and different scenarios can be envisaged for the sharing of the channel estimates (e.g., direct broadcasting from the RXs to all the TXs, sharing through a backhaul, …) [KG13]. In particular, the use of hierarchical (or layered) quantization is particularly adapted to the CSI feedback [NGG09]. The direct broadcasting of the CSI is studied in Subsection 2.4 in the case where a simple and practical digital quantizer is used.

Distributed precoding

Based on its individual CSIT, each TX designs its transmit coefficients. We focus here on the CSI dissemination problem under a conventional precoding framework. Hence, we assume that the sub-optimal zero forcing (ZF) precoder is used. Based on its own channel estimate$\mathbf{H}^{(j)}$, TX j computes then the ZF beamforming vector $\boldsymbol{t}_i^{(j)}$, to transmit symbols_i such that

$$\boldsymbol{t}_i^{(j)}, \triangleq \frac{\sqrt{P}\left(\mathbf{H}^{(j)}\right)^{-1}\mathbf{e}_i}{\|(\mathbf{H}^{(j)})^{-1}\mathbf{e}_i\|}. \tag{2.25}$$

Although a given TX j may compute the whole precoding matrix $\mathbf{T}^{(j)}$, only the j-th row is of practical interest. Indeed, TX j transmits solely $\mathrm{x}_j = \boldsymbol{e}_j^{\mathrm{H}}\mathbf{T}^{(j)}\boldsymbol{s}$. The effective multi-user precoder T verifies then

$$\mathbf{x} = \mathbf{T}\mathbf{s} = \begin{bmatrix} \mathbf{e}_1^{\mathbf{H}}\mathbf{T}^{(1)} \\ \mathbf{e}_2^{\mathbf{H}}\mathbf{T}^{(2)} \\ \vdots \\ \mathbf{e}_K^{\mathbf{H}}\mathbf{T}^{(K)} \end{bmatrix} \boldsymbol{s}. \tag{2.26}$$

Finally, we denote by $\mathbf{T}^{\star} = [\boldsymbol{t}_1^{\star}, \cdots, \boldsymbol{t}_K^{\star}]$the precoder obtained with perfect CSI at all TXs. It then verifies

$$\boldsymbol{t}_i^{\star} \triangleq \frac{\sqrt{P}\,(\mathbf{H})^{-1}\mathbf{e}_i}{\|(\mathbf{H})^{-1}\mathbf{e}_i\|}. \tag{2.27}$$

Optimization of the CSIT allocation

Optimizing directly the allocation of the number of bits at finite SNR represents a challenging problem which gives little hope for analytical results. Instead, we identify one CSIT allocation solution achieving the same DoF as under the fully shared CSIT setting.

Definition*(DoF achieving CSIT allocation):* We define the set of DoF-achieving CSIT allocations $\mathbb{B}_{\mathrm{DoF}}(\mathbf{\Gamma})$ as

$$\mathbb{B}_{\mathrm{DoF}}(\mathbf{\Gamma}) \triangleq \left\{\left\{\mathbf{B}^{(j)}\right\}_{j=1}^{K} | \forall i, \mathrm{DoF}_i\left(\left\{\mathbf{B}^{j}\right\}_{j=1}^{K}, \mathbf{\Gamma}\right) = 1\right\}. \quad (2.28)$$

Hence, an interesting problem consists in finding the minimal CSIT allocation (where minimality refers to the size provided above) which achieves the maximal generalized DoF at every user:

$$\underset{\left\{\mathbf{B}^{(j)}\right\}_{j=1}^{K}}{\mathrm{minimize}}\, s\left(\left\{\mathbf{B}^{(j)}\right\}_{j=1}^{K}\right) \text{ subject to } \left\{\mathbf{B}^{(j)}\right\}_{j=1}^{K} \in \mathbb{B}_{\mathrm{DoF}}(\mathbf{\Gamma}). \quad (2.29)$$

In this paper, we focus on an "achievability" result, by exhibiting a CSIT allocation that achieves the maximal DoF while having a much lower size than the conventional (uniform) CSIT allocation. Furthermore, the proposed "achievable scheme" will prove to have particularly interesting properties, which distinguish it from other solutions in the literature (e.g., clustering). The problem of finding a minimal-size allocation policy while guaranteeing full DoF (i.e. DoF equal to the perfect CSIT case) is an interesting problem, but an extreme challenging one, which, to our best knowledge, remains open.

2.3.3 Preliminaries: The conventional CSIT Allocation

In order to properly understand the theoretical results provided in the next subsection, a first step consists in discussing the solution of reference which would be used in the literature. This reference CSIT allocation will be denoted from now on as the "conventional" CSIT allocation. It corresponds to conveying to each TX the CSI relative to thefull multi-user channel, enabling all the TXs to do the same processing and compute a common precoder $\mathbf{T}^{(j)} = \widehat{\mathbf{T}}, \forall j$.

Proposition*(Conventional CSI Allocation):* Considering the generalized DoF model presented above with $\sigma_{k,i}^2 = P^{-\Gamma_{k,i}}$, let us define "*conventional*" CSIT allocation as

$$\left\{\mathbf{B}^{\mathrm{conv},(j)}\right\}_{k,i} \triangleq \left\lceil 1 - \Gamma_{k,i} \right\rceil^{+} \log_2(\mathrm{P}), \forall k, i, j. \quad (2.30)$$

Then:

$$\left\{\mathbf{B}^{\mathrm{conv},(j)}\right\}_{j=1}^{K} \in \mathbb{B}_{\mathrm{DoF}}. \quad (2.31)$$

This CSIT allocation provides to each TX the K channel vectors relative to the K RXs. Theterm $\Gamma_{k,i}$ corresponds to the effect of the variance of the channel element $H_{k,i}$(equal to $\sigma_{k,i}^2 = P^{-}\Gamma_{k,i}$) following well known results of rate-distorsion theory[CT06]. This means that each TX requiresa number of channel estimates growing unbounded with K. This represents a serious issue in large/dense networks which prompts designers, in practice, to restrict cooperation to smallcooperations clusters. This conventional CSIT allocation corresponds in fact to the allocation of "full" multi-user CSI to all the TXs. We will now show that this full allocation is not efficient and that large savings in CSIT sharing can be realized without any performance reduction.

2.3.4 Distance-based CSIT Allocation

Before stating our main result, we first define the notion of shortest path which will be needed for the theorem.

Definition*(Shortest path):* We define a path from TX j to RX k as the tuple $(\mathrm{a}_1, \cdots, \mathrm{a}_n)$with $a_i \in \{1, \ldots, K\}$ being the index of a TX/RX pair and $\mathrm{a}_1 = j$ and $\mathrm{a}_n = k$. Given the interference level matrix $\mathbf{\Gamma}$, the length $\mathrm{L}(\mathrm{a}_1, \cdots, \mathrm{a}_n)$ of a path is then given by

$$\mathrm{L}(\mathrm{a}_1, \cdots, \mathrm{a}_n) \triangleq \sum_{i=1}^{n-1} \Gamma_{a_{i+1};a_i}. \tag{2.32}$$

We can then define the shortest path from TX j to RX k, which we denote by $\Gamma_{j\to k}$, in the sense that

$$\Gamma_{j\to k} \triangleq \min_{(\mathrm{a}_2,\cdots,\mathrm{a}_{n-1})} \mathrm{L}(\mathrm{j}, \mathrm{a}_2, \cdots, \mathrm{a}_{n-1}, k). \tag{2.33}$$

Example: Let us consider the shortest path $\Gamma_{1\to 3}$in a network with 3 TX/RX pairs. Keeping in mind that $\boldsymbol{\Gamma_{i,i}} = 0$, ∀i, it is then simply equal to

$$\Gamma_{1\to 3} = \min(\Gamma_{3,2} + \Gamma_{2,1}, \quad \Gamma_{3,1}). \tag{2.34}$$

We can now state our first main result.

Theorem*(Distance-based CSI Allocation):* Let us define the distance-based CSIT allocation as

$$\left\{\mathbf{B}^{\mathrm{dist},(j)}\right\}_{k,i} \triangleq \left[1 - \Gamma_{k,i} - \gamma_{k,i}^{(j)}\right]^{+} \log_2(\mathrm{P}) \,, \forall k, i, j. \tag{2.35}$$

Then:

$$\left\{\mathbf{B}^{\mathrm{dist},(j)}\right\}_{j=1}^{K} \in \mathbb{B}_{\mathrm{DoF}}. \tag{2.36}$$

If the interference level matrix $\boldsymbol{\Gamma}$ tends to the zero matrix $\mathbf{0}_{K\times K}$, there is then no attenuation of the interference due to the pathloss and the distance-based CSIT allocation converges as expected to the conventional CSIT allocation. More generally, the distance-based CSIT allocation exploits the fact that if two TX/RX pairs interfere only through weak channels, they need to exchange a small amount of CSI.

Remark: If the interference level matrix is a symmetric matrix, the expressions simplify such that

$$\gamma_{k,i}^{(j)} = \min(\Gamma_{k\to j}, \quad \Gamma_{i\to j}). \tag{2.37}$$

Another interesting case arises if the interference level matrix satisfies that

$$\Gamma_{k,j} \leq \Gamma_{k,i} + \Gamma_{i,j} \,, \forall i, j, k. \tag{2.38}$$

It then holds that

$$\Gamma_{k\to j} = \Gamma_{j,k}. \tag{2.39}$$

In particular, this last condition, which is some form of triangular inequality, is satisfied when the long term attenuation introduces a notion of *distance* between the TX/RX pairs. This is the case in a wireless network with a regular pathloss attenuation.

2.3.5 Simulation Results

We verify now by simulations that the maximal DoF per user is achieved by the distance-based CSIT allocation. At the same time, we compare the distance-based CSIT allocation to the CSI disseminations commonly used, i.e., uniform CSIT allocation and clustering.

We consider the conventional wireless model with an attenuation coefficient $\varepsilon = 2$and a transmit power equal to P_0= 30dB and the interference-level matrix $\boldsymbol{\Gamma}$ is obtained from these two parameters. Note that we consider only $d_{i,j} > 1$(where $d_{i,j}$represents the distance between TX $j$and RX i) to ensure that the interfering links are weaker than the direct links. We use Monte-Carlo averaging over 1000 channel realizations.

In a first step, we study a network with a regular geometry where $K = 36$ TX/RX pairs are placed at the integer values inside a square of dimensions 6×6. We show in Figure 5the average rate achieved with different CSIT allocation policies. Specifically, the distance-based CSIT allocationis compared to two alternative CSIT allocations, being the uniform CSIT allocation $\{\mathbf{B}^{\mathrm{unif},(j)}\}_{j=1}^{K}$where the bits are allocated uniformly to the TXs, and the clusteringone, denoted by $\{\mathbf{B}^{\mathrm{cluster},(j)}\}_{j=1}^{K}$,for which (non-overlapping) regular clustering of size 4 is used. Both CSIT allocations are chosen to have the same size as the distance-based one:

$$s\left(\{\mathbf{B}^{\mathrm{unif},(j)}\}_{j=1}^{K}\right) = s\left(\{\mathbf{B}^{\mathrm{cluster},(j)}\}_{j=1}^{K}\right) = s\left(\{\mathbf{B}^{\mathrm{dist},(j)}\}_{j=1}^{K}\right). \tag{2.40}$$

With these parameters, the size of the distance based CSIT allocation is only equal to 9% of the size of the conventional CSIT allocation. Nevertheless, it can be observed to achieve the maximal generalized DoF while the clustering solution has a smaller slope. The distance-based CSIT allocation suffers from a strong negative rate offset. However, this offset is a consequence of our analysis being limited to the high SNR regime and can be also observed in the fact that clustering outperforms ZF based on the conventional CSIT-allocation, which represents in fact the true reference for our scheme. Indeed, using ZF with many users is very inefficient at intermediate SNR, particularly in a network with strong pathloss. Furthermore, the number of TX/RX pairs K which is here relatively large, has not been taken into account. Hence, this strong negative rate offset can be easily reduced by optimizing the precoding scheme and the CSIT allocation at finite SNR. The key element being that the distance-based CSIT allocation does not present the usual limitations of clustering, i.e., edge-interference and bad scaling properties as the size of the cluster increases.

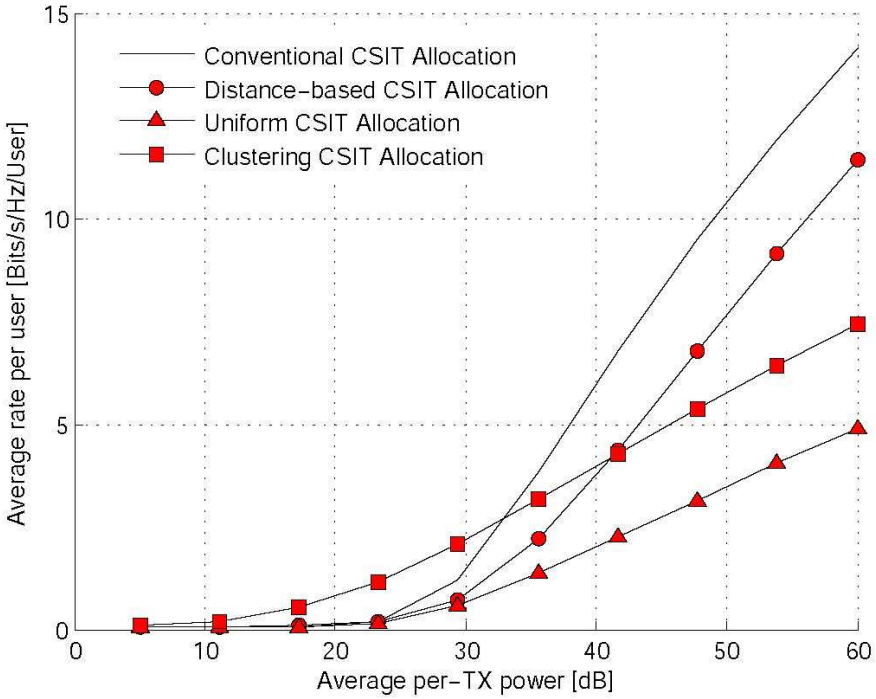

Figure 5: Average rate per user as a function of the per-TX power for K = 36. The 3 limited feedback CSIT allocations used have the same size which is equal to 9% of the size of the conventional CSIT allocation.

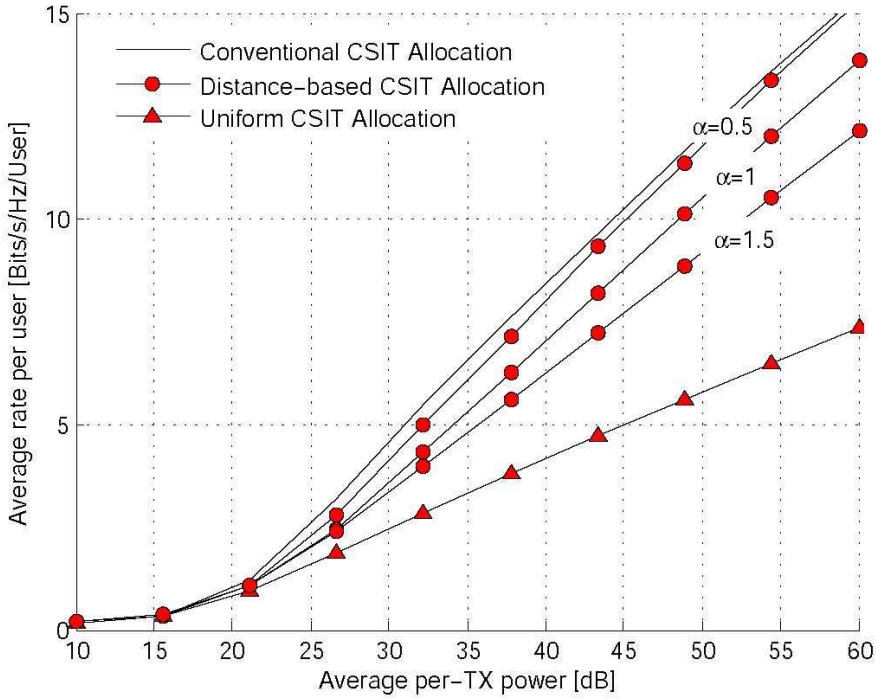

Figure 6: Average rate per user as a function of the per-TX power for K = 15 for the polynomial pathloss attenuation. The CSIT allocation uses respectively 39%, 17%, and 13% of the size of the conventional CSIT allocation.

Finally, we show in Figure 6 the average rate per user in a network made of $K = 15$ TX/RX pairs being located uniformly at random over the same square of dimensions 6×6. To verify the impact of allocating more –or less– CSIT, we compare the average rate achieved with the distance-based CSIT allocation to the average rate obtained if we use the following variation of the CSIT allocation:

$$\left\{\mathbf{B}^{\mathrm{dist},(j)}\right\}_{k,i}(\alpha) \triangleq \left[1 - \Gamma_{k,i} - \alpha\gamma_{k,i}^{(j)}\right]^{+} \log_2(\mathrm{P}) \,, \forall k,i,j \qquad (2.41)$$

This allows to observe the impact of reducing $(\alpha > 1)$ or increasing $(\alpha < 1)$the CSIT compared to the distance-based CSIT allocation.

We can observe that reducing the CSIT allocation leads to reducing the slope, i.e., the DoF, while using more feedback bits leads to a vanishing rate offset. This is in agreement with our theoretical result that the distance-based CSIT allocation leads to a finite (bounded) rate offset.

2.3.6 Discussion of the results

We have discussed the problem of optimizing the CSIT dissemination in a network MIMO scenario. In particular, following a generalized DoF analysis, we have exhibited a CSIT allocation which allows to achieve the optimal generalized DoF while restricting the cooperation to a local scale. This behavior is critical for the cooperation of a large number of TXs to be practical.

The proposed CSIT allocation appears as an alternative to clustering where the hard boundaries of the cluster are replaced by a smooth decrease of the cooperation strength. Our focus has been on the high SNR performance, and the distance-based CSIT allocation should be further optimized to lead to gain in realistic transmissions. Yet, it appears to have a strong potential as an alternative to clustering. In addition, we have considered only the CSIT requirements in order to achieve global interference management. The design of feedback schemes and backhaul links allowing to achieve these requirements represents another very interesting research area. This work shows

that the CSIT requirements do not have to scale unbounded with the size of the network, which differs from the conclusions of several works from the literature. This is a consequence from letting the pathloss increase with the SNR, which makes the pathloss non-negligible at high SNR. We believe that this is the proper modelization of the pathloss in order to keep the impact of the network geometry, which, in contrast, becomes negligible in a DoF analysis with fixed pathloss.

2.4 Broadcast Channel Feedback in Cooperated Multiple Antenna Systems

2.4.1 Problem Formulation

Since we are heading to a 'all connected' world, where there are more and more devices being part of wireless network, there is a need to develop new strategies for coordinated transmission from nearby transmitters to any device in order to avoid or manipulate interference [KG13]. In such a dense network, we propose a distance based user centric clustering of base stations and a subsequent broadcast feedback of the CSI.

In the first phase, each Base Station (BS) will find the neighbouring UEs. Hence each UE will have different set of neighbouring BSs. This can be accomplished by BSs measuring the pathloss of different UEs in the neighbourhood using the location information. Then these BSs will send pilot signals for UEs to estimate the channels. Each UE will estimate channels from a neighbourhood of BSs. In the case of dense heterogeneous networks channel estimation has to be orthogonal since there can be pilot contamination. In such a case, we claim that, using broadcast feedback [KOT14] does not require any additional resources but gives a scalable feedback allocation.

The main highlight of broadcast feedback is that it is leading to a distributed CSI allocation depending on UE location, each BS can have CSI from a different set of UEs in the neighbourhood. We are using JP-CoMP and hence we assume that the data of UEs are shared among the BSs. When the system is of low mobility, there are many ways to have data sharing, for eg. using distributed caching. But needless to say, we can use interference alignment strategies or coordinated scheduling along with broadcast feedback, where the data sharing is not required.

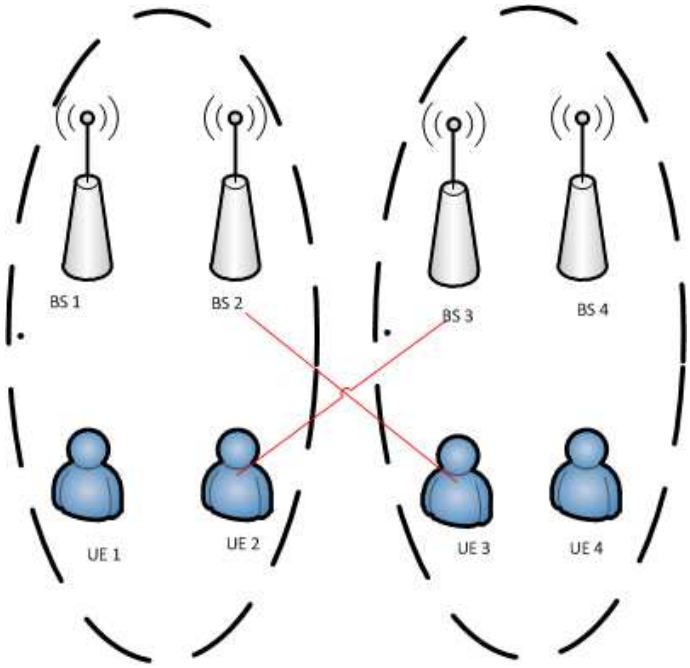

Figure 7: A toy example illustrating the network of interest, with 4 Base Stations (M=4) each with two antennas (J=2) serving 4 UEs (K=4).

Our current work [KOT15] is focusing on the precoder optimization in such a system where the CSI is distributed [KG13]. A classical limitation of CoMP clustering is the degradation created by inter-cluster interference which is left untreated by cooperation mechanisms within the cluster. This degradation is particularly severe in smaller cluster sizes (2 or 3 cells), while it is desirable to maintain clusters small in order to reduce feedback requirements. We propose a feedback and cooperation architecture which addresses this problem. We point out that the broadcast feedback scheme often leads to BS decoding the CSI feedback of additional users that do not end up being admitted in the cluster of users served by this BS, for instance because the same CSI is also received by other BS that are closer to the user. In previous cluster-based cooperation techniques, this extra CSI information available at the BS is not suitably exploited. We propose a scheme allowing to capitalize on this possible extra feedback in an opportunistic manner. This leads to a challenging decentralized MIMO precoding problem whose general solution is still open. Subsequently we propose a heuristic method that is built on the known notion of interference leakage. The new algorithm hence strikes a compromise between minimizing within-cluster and out-of-cluster interference that provides substantial gain over classical precoders ignoring inter-cluster interference. The preeminent feature and advantage of our method is that the computation of precoders at each base station is completely decentralized.

All the mathematical equations and its derivation including the main distributed precoding algorithm can be found in the paper [KOT15] which will be published soon.

2.4.2 Performance of Opportunistic Precoder

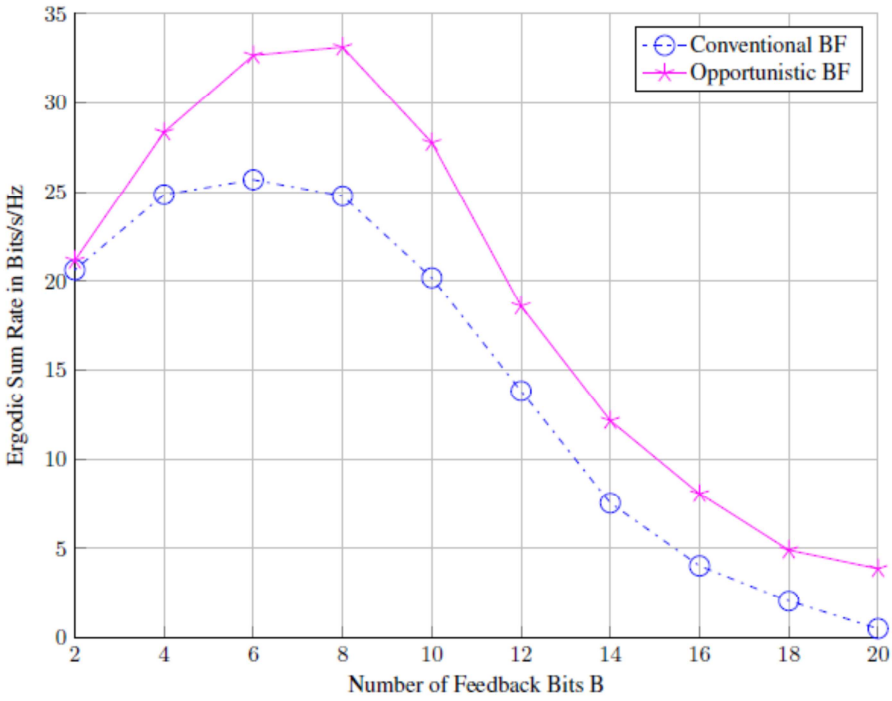

Figure 8: Variation of Sum Rate with Number of Feedback Bits B.

We compare the performance of the new opportunistic precoding algorithm with conventional precoding approach (ZF in each cluster of network MIMO) in Figure 8 for various amounts of feedback quantization bits B. As it can be seen, when the number of bits gets large, BSs receive a more accurate feedback but fewer BSs are able to actually decode it, which leads to performance decrease. Conversely, when the number of quantization bits B becomes too small, most BSs can decode the feedback, leading to wider cooperation clusters, albeit with poor CSI quality. This is the same behaviour for the ZF beamformer (conventional) and opportunistic beamformer.

2.4.3 **Conclusions**

We proposed a decentralized precoding method which is capable of exploiting additional opportunistic out-of-cluster broadcast feedback in Network MIMO. The method shows clear gain over a conventional network MIMO setup which exploits CSI limited to its own cluster. This decentralized precoding can also be applied for any case of distributed CSI, not just for the case of broadcast feedback.

3 NEW ADVANCED MIMO SCHEMES AND COMP CONCEPTS

3.1 Advanced Scheduling for intra and inter-site CoMP

3.1.1 Introduction

CoMP aims at improving the quality of service of users at cell edge (which answers to the above mentioned "anywhere" requirement). Indeed, users located at cell edge experience both lower received signal power and increased inter-cell interference compared to those at cell centre. Cooperation between adjacent cells can mitigate these issues. Many schemes can be considered for this purpose, but here only the Joint transmission (JT) DL CoMP scheme will be considered. The motivation for this choice is that this scheme (based on Single Frequency Networking) has the best Signal to Interference and Noise (SINR) improvement at the receiver. This gain will be accessible on the condition of ensuring perfect (time- and frequency-) synchronization between the cells involved in the CoMP process. This leads to a rapid exchange of data between cooperating cells. One of the blocking points of the CoMP-deployment in the current network is the need to deploy a Backhaul Network Fiber. In this context two main CoMP deployment strategies can be considered: either the cooperating cells belong to the same site (in which case no fiber will be necessary) or the cooperating cells belong to different sites i.e. not geographically co-located sites (in which case the fiber will be necessary). Considering the fact that a UE can be CoMP UE or not, UE set can be divided into two sub-sets: CoMP UEs and no CoMP UEs. Contrary to the usual case the same scheduler (located in an eNB or not) has to manage COMP UEs as well as no COMP UEs with fairness between these two UEs sub-sets. Moreover a CoMP UEs requires two times more resources blocks (sub-carriers) than a no CoMP UE. These different aspects have to take into account to propose a new Advanced Scheduling for CoMP.

3.1.2 Problem description

Once the serving cell has been selected a UE is CoMP candidate UE (CCUE) when its Reference Signal Received Power (RSRP) difference between serving cell and other cells satisfies a threshold requirement ($\boldsymbol{\Delta_P}$), e.g.

$$\mathrm{RSRP}_{\mathrm{UE\_k,serving\_cell}}\mathrm{RSRP}_{\mathrm{UE\_k,Cell\_i}} < \boldsymbol{\Delta_P} \quad (3.42)$$

If the condition is not met the UE becomes no-CoMP UE (nCUE) and it will not take benefit of SINR improvement brought by CoMP (Coherent JT is here assumed) throughout the transmission duration. CCUE becomes CoMP UE (CUE) at the resource block allocation accomplished by the scheduler (if resources block needed to process to CoMP are available at the two cells involved in the CoMP process) and if the performance gain could be achieved by CoMP). Thus, the scheduler must take into account two sets of UEs: the CCUEs and the nCUEs. A lot of deployment scenarios could be considered: inter-site cooperation, intra-site cooperation, 3GPP scenario 2 and full cooperation scenario. For last scenarios (inter-site for example) CoMP requires close coordination between geographically separated eNBs. Two types of scheduler are considered as shown in Figure 9:

- **Distributed scheduler:** For distributed scheduling, the decision unit is located for each UE at the primary cell. Resource availability requests are sent to the secondary cell. The secondary cell responds to these requests and waits for resource reservation.
- **Centralized scheduler:** For centralized scheduling, the decision unit is located at a single geographic location of the CoMP cluster. No resource availability request is necessary (as the secondary cell is part of the CoMP cluster). But this kind of scheduler requires the data flow from all the cells of the CoMP cluster to a single decision unit.

For the two schedulers the backhaul bandwidth consumption will be more important when the number of CoMP UEs is high and/or when the CoMP cluster is large. The feasibility of these schedulers may be considered for the small size clusters. The larger CoMP cluster size, the

larger the amount of information exchanged between cells: CoMP cluster size greater than 9 cells seems to be unrealistic at present.

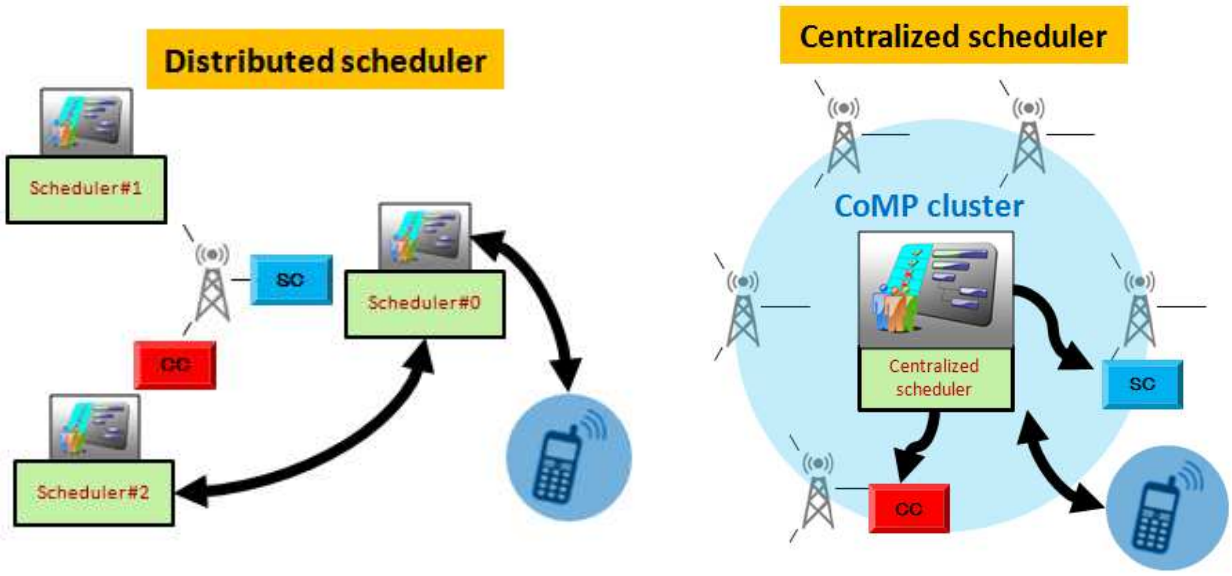

SC = Serving Cell CC = Collaborative Cell

Figure 9: Two scheduling approach for CoMP.

For the distributed scheduling the resource block allocation has to be performed per cell in parallel (the risk of the resource access conflict is high and is often difficult to manage) while the centralized scheduler allocates the resource per CoMP cluster (this type can better manage the resource access conflict).

Considering the fact that two UEs populations (nCUEs and CCUEs) have to be scheduled, two strategies were proposed for the distributed scheduling:

- Successive scheduling with prioritization: A strict prioritization is performed. CCUEs over nCUEs then the controversy.
- Simultaneously scheduling: The scheduling is only based on Proportional Fairness (PF) metric without any other consideration.

For these two strategies and depending on the resource block availability on the serving cell an nCUE will be served or not. At the beginning of a transmission cell a CCUE will become:

- a served CUE (CoMP UE) if resource block on primary (or serving) cell and on secondary cell are available
- a served nCUE if only the resource block on the primary cell are available
- or stays CCUE if else

During the transmission the UE status stays the same (a CUE cannot become an nCUE and vice versa).

To analyze the performance of such a scheduler, a transfer function was proposed. The CoMP transfer function (see Figure 10) gives the throughput by enabling the CoMP feature according throughput without enabling this CoMP feature for every UE:

- a point on the right slope unit corresponds to a UE without CoMP improvement
- a point below the line, to a UE that undergoes a performance degradation

- and in the above, to a UE that undergoes a performance improvement.

As shown in the figure the improvement of the CoMP performances is made to the detriment of the legacy UEs.

The goal here is to treat the weakness of this scheduler (highlighted by Figure 10) through a centralized opportunistic approach (to introduce more fairness between the CCUEs and nCUEs).

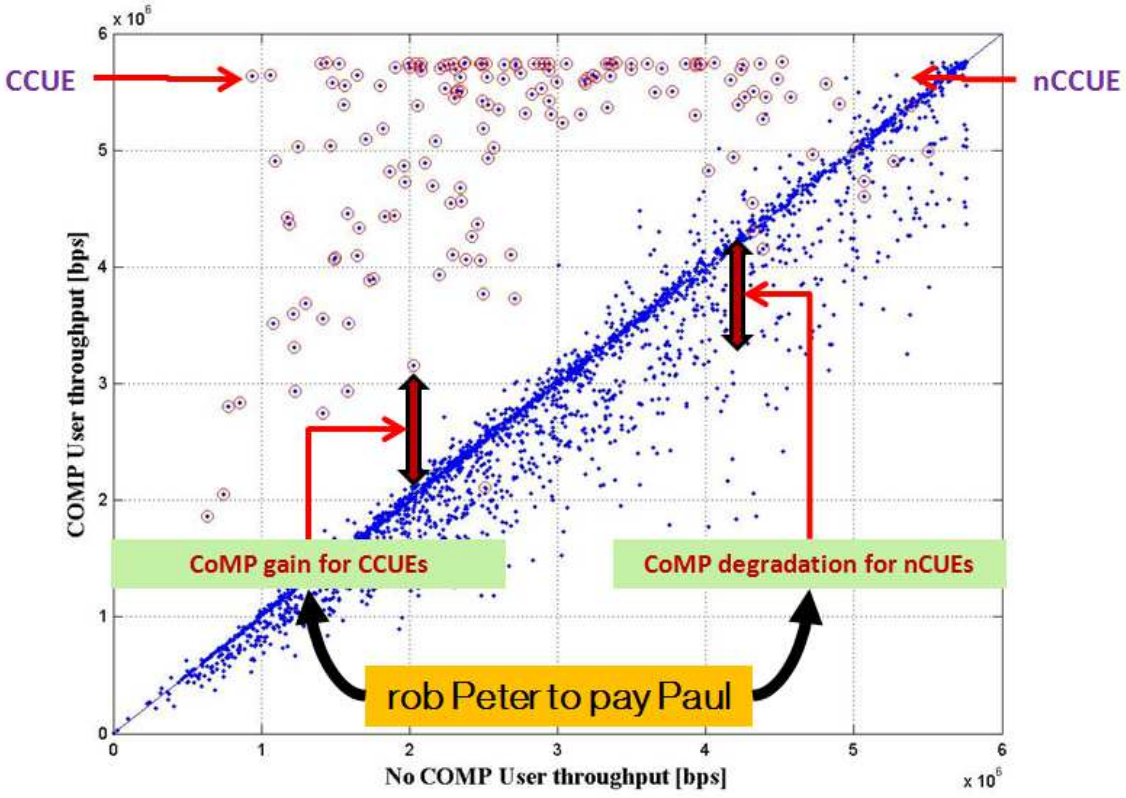

Figure 10: Weakness of the studied scheduler.

3.1.3 Opportunistic scheduling approach

The idea of the opportunistic scheduling approach is first of all to achieve at least the performances of no CoMP. CCUEs will be served as CUEs only if the resources are available otherwise it will be served as an nCUE. The information coming from the UEs is centralized and handled by a unique scheduler that takes the decisions.

The opportunistic scheduler has 3 steps:

- By assuming that all the UEs are nCUEs (as would be the case if the CoMP feature has not been activated) the purpose of this first step is to ensure minimum performance for the nCUEs.
- The second step is to select the CCUEs that are expected to yield gains if the CoMP feature is enabled. For this a set of needed information is sent to a second level centralized unit that will treat all CCUEs. The remaining CCUEs will be considered as nCUEs.
- The final step is to assess the schedulable ability of the retained CCUEs. CCUE that cannot be served as a CUE will become nCUE otherwise they become CUE.

Figure 11 illustrates the operation of the successive and opportunistic schedulers:

- In the first step, the successive scheduler tries to serve all CCUEs (at the end of this step only 6 CCUEs will be served). Considering the opportunistic scheduler, the UEs

are not treated as CCUE, as if as CoMP feature was not enabled (at the end of this step 12 UEs could be served).

- In the case of the successive scheduling the second step is to use the available resource blocks to serve the nCUEs (at the end of this step only 3 nCUEs will be served). In the case of the opportunistic scheduling, only the CCUEs are considered and CCUE will become CUE if the necessary resources blocks are available (in the exemple only 2 CCUEs become CUEs).

The result will be:

- Successive scheduling: 9 UEs are served: 3nCUEs and 6 CCUEs.
- Opportunistic scheduling: 12 UEs are served: 10 nCUEs and 2 CCUEs.

By respect to this example it is clear that the number of served UEs in the case of a opportunistic scheduling will be equal to the number of served UEs if the CoMP feature is not activated.

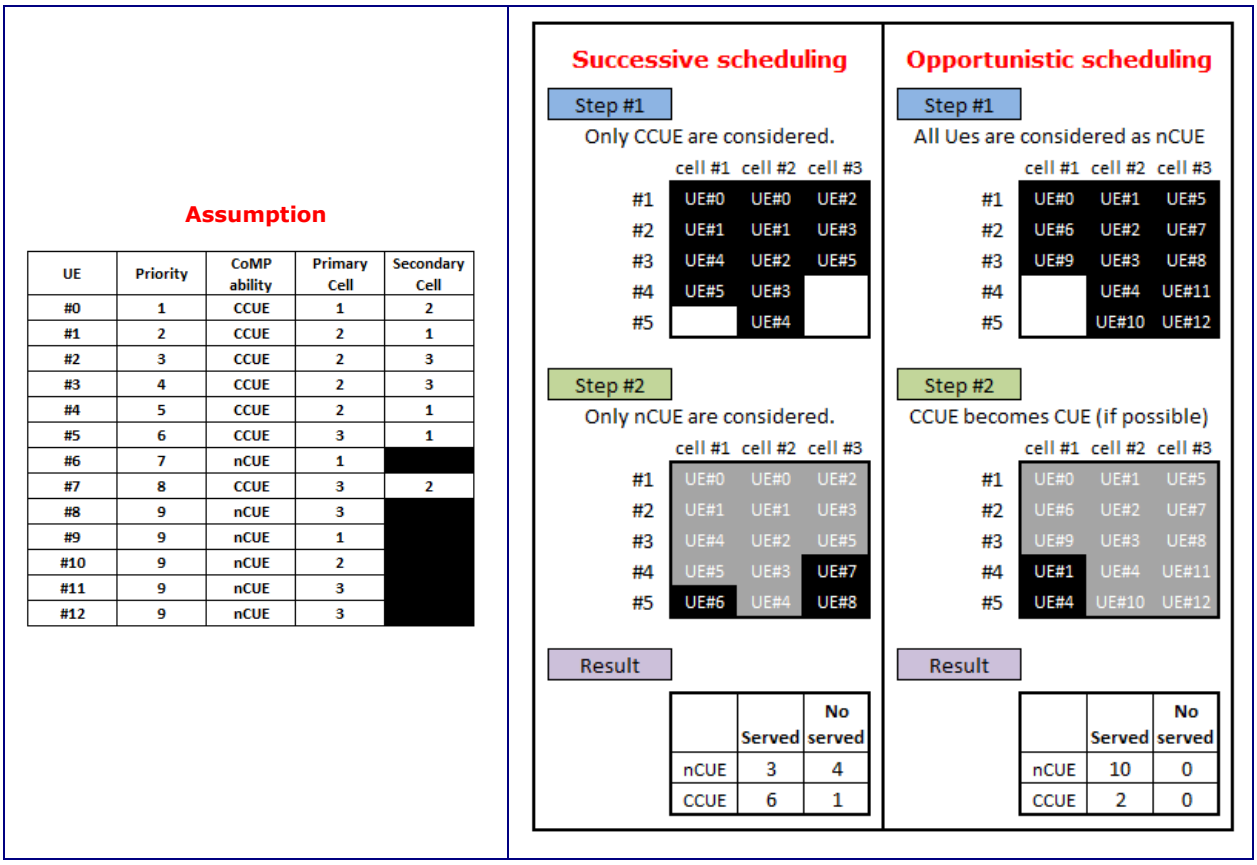

UE	Priority	CoMP ability	Primary Cell	Secondary Cell
#0	1	CCUE	1	2
#1	2	CCUE	2	1
#2	3	CCUE	2	3
#3	4	CCUE	2	3
#4	5	CCUE	2	1
#5	6	CCUE	3	1
#6	7	nCUE	1	
#7	8	CCUE	3	2
#8	9	nCUE	3	
#9	9	nCUE	1	
#10	9	nCUE	2	
#11	9	nCUE	3	
#12	9	nCUE	3	

Figure 11: Principle of operation of the two schedulers.

3.1.4 Performance assessment

The issue addressed in the following section is to evaluate the system performance gain obtained with the proposed scheduler.

3.1.4.1 *CoMP scenarios*

Two scenarios are considered: Intra-site and Full cooperation. Intra-site cooperation consists in 3 cells of the same site. In the case of Full cooperation all the network is a CoMP cluster.

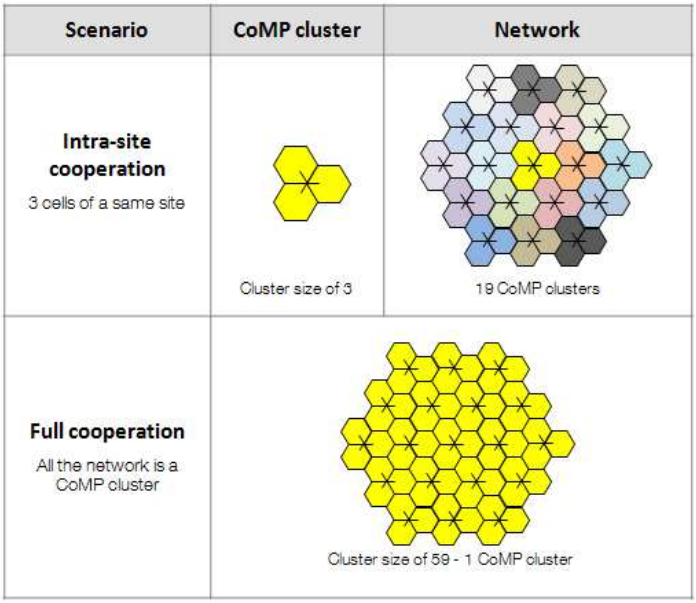

Figure 12: CoMP scenarios.

The benefit of the first CoMP cluster is that no black fiber is needed. The need to deploy a Backhaul Network Fiber increases with the CoMP cluster size. Notice that Full cooperation is an unrealistic case but performances obtained in this case correspond to upper bound performance.

3.1.4.2 *Scheduling transfer function*

Figure 13 shows the CoMP transfer function in the case of the opportunistic scheduler (that shows the throughput when activating the CoMP function with the opportunistic scheduling).

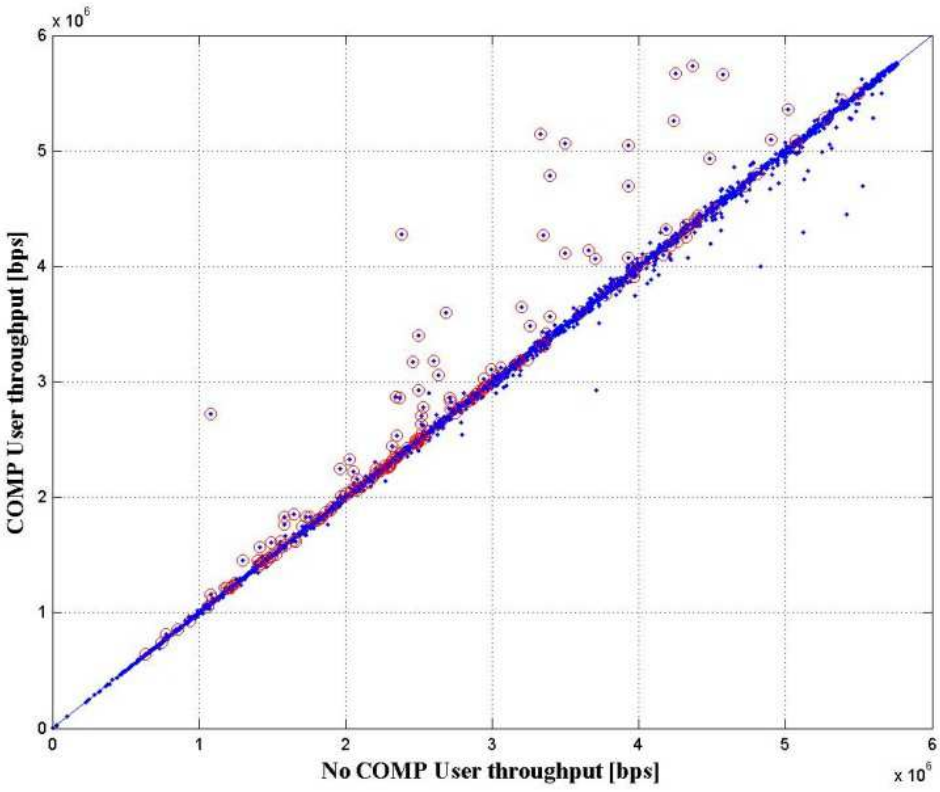

Figure 13: CoMP transfer function in the case of the opportunistic scheduler.

As shown on the figure, the opportunistic approach is a better tradeoff between offering CoMP opportunities and degrading legacy UEs QoS. Less UEs are served as CoMP but there are not anymore degraded UEs.

3.1.4.3 *System performance*

The following figures show the performance obtained with the opportunistic scheduler in term of:

- Cell edge (5%),
- Cell average (50%),
- And sum rate.

These gains were obtained for different threshold values (Δ_P). The percentage of CCUEs for different values of Δ_P increases with Δ_P. For Δ_P =21dB, 100% of the UEs are CCUEs.

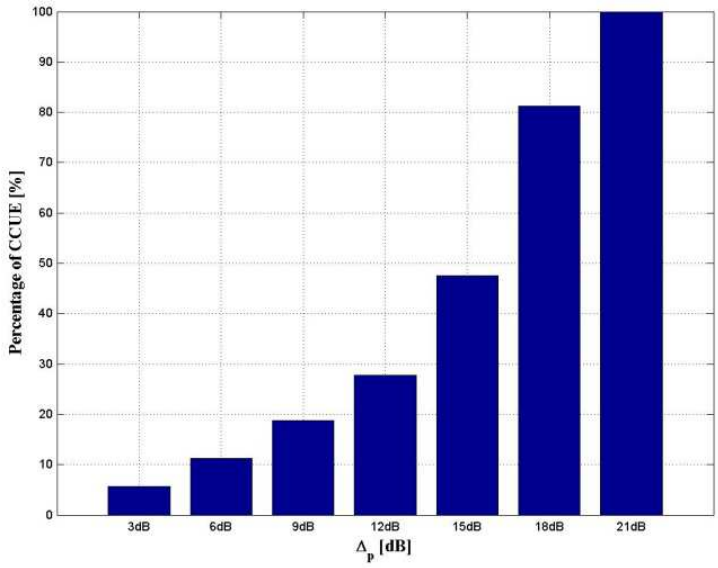

Figure 14: Impact of threshold requirement on CCUES number.

Δ_P has 2 antagonist effects:

- at one side the number of CCUEs increase (so a lot of UEs will take benefice of CoMP)
- But on another side the complexity of CoMP increases too (as for a moment each UE can be CUE).

Figure 15 shows the performance improvement for intra-site cooperation. The gain increases when the threshold increases and has a maximum for a threshold of 15 dB.

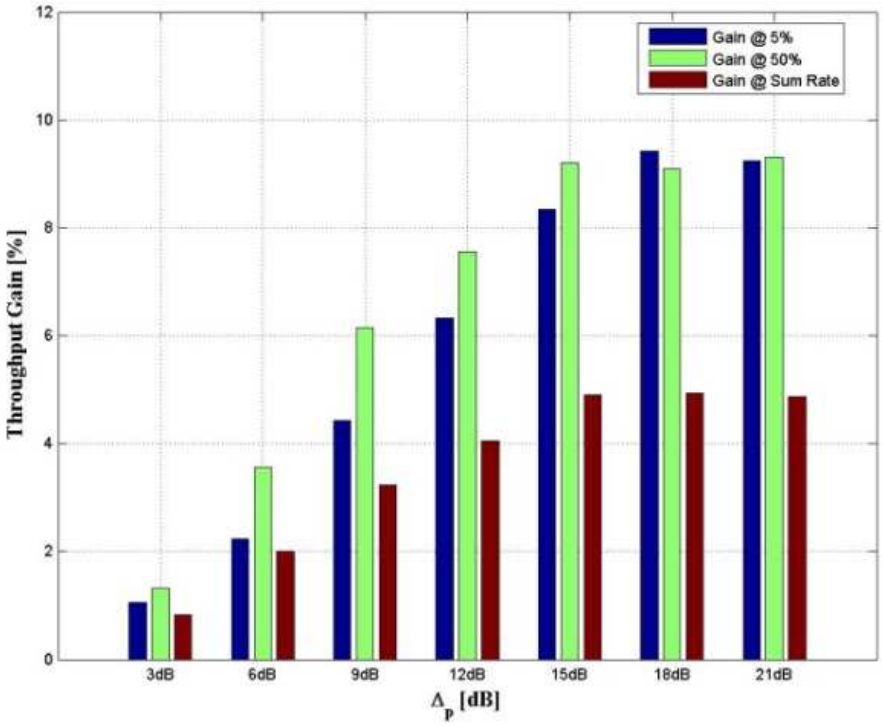

Figure 15: Intra-site cooperation system performance.

Figure 16 shows the performance improvement for full cooperation. Obviously the smaller the coordinating cluster size, the smaller the throughput gains. By respect to the previous case the performance improvement could be explained by the fact that 56% of CCUES in the case of full cooperation will no longer CCUES in intra-site cooperation.

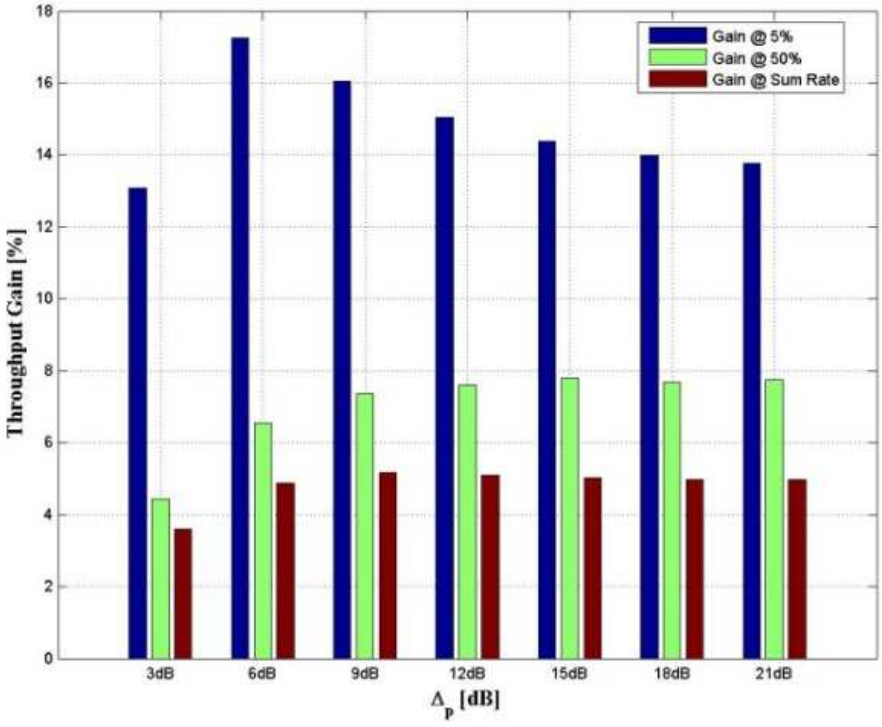

Figure 16: Full cooperation system performance.

The scheduling policy has a strong impact on the performance of CoMP. An opportunist approach allows interesting gains at cell edge without impacting system capacity and legacy UEs throughput. One of the important parameters that affect system performance is undoubtedly the size of the CoMP cluster. This can be explained by the existence of line of sight channel condition in the ITU channel model.

3.2 Downlink Multi-user CoMP with Interference Aware Receiver

In this study, we focus on CoMP, and Multi-User MIMO (MU-MIMO), that were introduced in LTE-A in order both to improve cell edge users quality of service, and to increase cell spectrum efficiency. We use them jointly, and study their performance when used with a user terminal whose receiver has interference rejection capability. In this context, four interference aware receivers are studied, which cover the three categories of Network-Assisted Interference Cancellation receivers defined in [TR36.866]: Interference Suppression (IS), Maximum Likelihood (ML), and Interference Cancellation (IC) receivers. In this first step, these receivers performance are compared assuming perfect knowledge of interference characteristics.

3.2.1 Signal model

Figure 17 shows the scenario of the study: the DL of a cellular network is considered. The UE of interest in the following is called UE0. UE1 and UE2 are scheduled on the same time and frequency resources as UE0. UE1 is associated to eNB1 whereas UE2 is associated to eNB2. UE0 benefits from the cooperation of both eNBs in Joint Processing / Joint Transmission (JP/JT) mode [TR36.814][TR36.819]. MU-MIMO Transmission Mode 5 (TM5), [TS32.213], is used with precoders defined by 3GPP in [TS136.211].

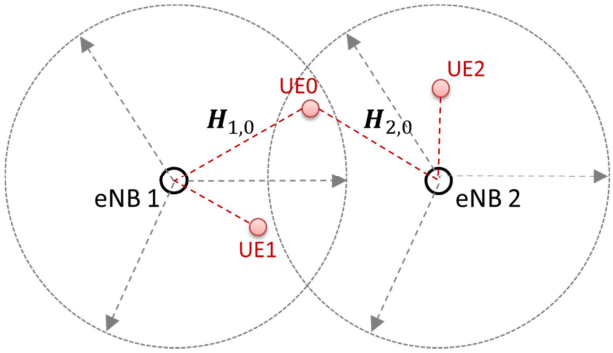

Figure 17: MU-MIMO CoMP scenario.

The following notations apply:

- $N_R \in \mathbb{N}^+$ is the number of receive antennas (at the UE side),
- $N_T \in \mathbb{N}^+$ is the number of transmit antennas (at the eNB side),
- $\boldsymbol{H}_{i,0} \in \mathbb{C}^{N_R \times N_T}, i \in \{1,2\}$ is the channel from eNBi to UE0,
- $\boldsymbol{w}_{i,j} \in \mathbb{C}^{N_T \times 1}, i \in \{1,2\}, j \in \{0,1,2\}$ is the precoder applied at eNBi for UEj,
- $x_i \in \mathbb{C}, i \in \{0,1,2\}$ are the data intended to UEi,
- $\boldsymbol{y} \in \mathbb{C}^{N_R \times 1}$ is the signal received at UE0,
- $\boldsymbol{z} \in \mathbb{C}^{N_R \times 1}$ is AWGN with variance N_0.

The signal received at UE0 can then be written as in (3.43).

$$\boldsymbol{y} = \boldsymbol{H}_{1,0}\left(\boldsymbol{w}_{1,1}x_1 + \boldsymbol{w}_{1,0}x_0\right) + \boldsymbol{H}_{2,0}\left(\boldsymbol{w}_{2,2}x_2 + \boldsymbol{w}_{2,0}x_0\right) + \boldsymbol{z} \qquad (3.43)$$

In order to highlight the interference term, (3.43) can be re-written as in (3.44). Here, the interference is represented by the second sum.

$$\boldsymbol{y} = x_0 \sum_{i=1}^{2} \boldsymbol{H}_{i,0}\boldsymbol{w}_{i,0} + \sum_{i=1}^{2} \boldsymbol{H}_{i,0}\boldsymbol{w}_{i,i}x_i + \boldsymbol{z} \tag{3.44}$$

3.2.2 Interference-Aware receivers

Interference-Aware (IA) receivers aim at detecting the useful data x_0 from the received signal $\boldsymbol{y}$ in (3.44), with various levels of knowledge of the interfering parameters (interfering precoders, constellations, power,…). Obviously the more parameters are available at the IA receiver side, the more signalling is required, decreasing the system throughput. A tradeoff must then be found between IA receivers' performances and signalling rate. In this study, as a first step, the performance of IA receivers with full knowledge of interfering precoders and constellations is assessed.

3.2.2.1 *Single Layer MMSE equalizer [BAI11]*

The effective channel $\boldsymbol{g}_e$ and interference channels $\boldsymbol{g}_i, i \in \{1,2\}$, are respectively defined as in (3.45) and (3.46).

$$\boldsymbol{g}_e = \sum_{i=1}^{2} \boldsymbol{H}_{i,0}\boldsymbol{w}_{i,0} \in \mathbb{C}^{N_R \times 1} \tag{3.45}$$

$$\boldsymbol{g}_i = \boldsymbol{H}_{i,0}\boldsymbol{w}_{i,i} \in \mathbb{C}^{N_R \times 1}, i \in \{1,2\} \tag{3.46}$$

The Single Layer (SL)-MMSE receiver $\boldsymbol{b}$ minimizes the mean square error w.r.t. the desired signal x_0. With perfect knowledge of (3.45) and (3.46), the SL-MMSE receiver can be obtained by minimizing the mean square error e, where:

$$\begin{aligned} e &= E\{\|\boldsymbol{b}^H\boldsymbol{y} - x_0\|^2\} \\ &= \left(\boldsymbol{b}^H - E_x\boldsymbol{g}_e^H\boldsymbol{R}_{\boldsymbol{y}}^{-1}\right)\boldsymbol{R}_{\boldsymbol{y}}\left(\boldsymbol{b}^H - E_x\boldsymbol{g}_e^H\boldsymbol{R}_{\boldsymbol{y}}^{-1}\right)^H + E_x\left(1 - E_x\boldsymbol{g}_e^H\boldsymbol{R}_{\boldsymbol{y}}^{-1}\boldsymbol{g}_e\right) \end{aligned} \tag{3.47}$$

With E_x the transmit signal energy, $\boldsymbol{R}_{\boldsymbol{y}} \in \mathbb{C}^{N_R \times N_R}$ the covariance matrix of the receive signal vector given by (3.48), $\boldsymbol{R}_{\boldsymbol{\eta}} \in \mathbb{C}^{N_R \times N_R}$ the covariance matrix of interference and noise vectors, given by (3.49) and $\mathrm{I}_{\mathrm{N_R}}$ the identity matrix of size $\mathrm{N_R} \times \mathrm{N_R}$.

$$\boldsymbol{R}_{\boldsymbol{y}} = E_x\boldsymbol{g}_e\boldsymbol{g}_e^H + \boldsymbol{R}_{\boldsymbol{\eta}} \tag{3.48}$$

$$\boldsymbol{R}_{\boldsymbol{\eta}} = E_x\sum_{i=1}^{2}\boldsymbol{g}_i\boldsymbol{g}_i^H + N_0\boldsymbol{I}_{N_R} \tag{3.49}$$

Finally, the minimum value of (3.47) is given by setting:

$$\boldsymbol{b}^H = \boldsymbol{b}_{SL-MMSE}{}^H = E_x\boldsymbol{g}_e^H\boldsymbol{R}_{\boldsymbol{y}}^{-1} \tag{3.50}$$

3.2.2.2 *Interference Rejection Combiner [BAI11]*

With perfect knowledge of (3.45) and (3.46), the Interference Rejection Combiner (IRC) receiver for detecting the desired signal x_0 can be represented as in (3.51).

$$\boldsymbol{b}_{IRC}{}^H = \frac{\boldsymbol{g}_e^H\boldsymbol{R}_{\boldsymbol{\eta}}^{-1}}{\boldsymbol{g}_e^H\boldsymbol{R}_{\boldsymbol{\eta}}^{-1}\boldsymbol{g}_e} \tag{3.51}$$

Both SL-MMSE and IRC receivers presented above are analytically equivalent [BAI11]. In the following, only the performances of SL-MMSE receiver will then be assessed.

3.2.2.3 *MMSE Absolute Interference Cancellation (AIC) receiver [GHA09]*

Authors in [GHA09] propose a low complexity algorithm for spatial interference cancellation in the presence of one strong interferer. Let us define the signal $\boldsymbol{y}_i$ and its estimate $\hat{\boldsymbol{y}}_i$ as in (3.52). $\boldsymbol{y}_i$ is the contribution of data of UEi in the interference. $\hat{\boldsymbol{H}}_{i,0}$ is the estimation of $\mathrm{H_{i,0}}$; it is supposed perfect in this study.

$$\begin{aligned} \boldsymbol{y}_i &= x_i \boldsymbol{H}_{i,0} \boldsymbol{w}_{i,i}, i \in \{1,2\} \\ \hat{\boldsymbol{y}}_i &= \hat{x}_i \hat{\boldsymbol{H}}_{i,0} \boldsymbol{w}_{i,i}, i \in \{1,2\} \end{aligned} \tag{3.52}$$

Figure 18 presents the scheme of the receiver with the notations above. The receiver estimates in parallel the interfering data $\hat{x}_i, i \in \{1,2\}$. In this study this stage is realized thanks to the SL-MMSE equalizer presented in section 3.2.2.1, adapted to the interfering data x_i. The interfering stream $\hat{\boldsymbol{y}}_i$ is then reconstructed and substracted from the received signal $\boldsymbol{y}$. The desired signal is finally estimated from this signal.

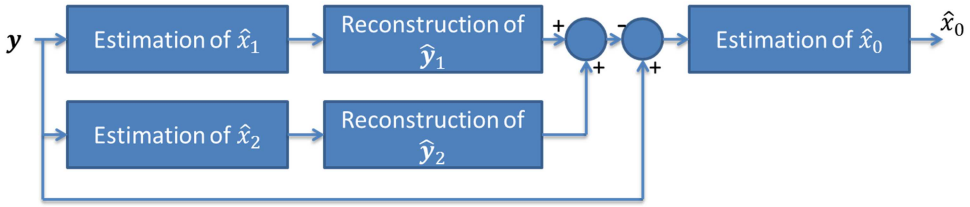

Figure 18: MMSE-AIC receiver with two interferers.

3.2.2.4 *Interference Aware Max Log MAP (IA-ML) receiver [GHA11]*

IA-ML receiver computes a reduced complexity Log Likelihood Ratio (LLR) for each received bit at UE0 which takes into account the structure of residual interference. Let us consider the following transmission structure at the eNB side:

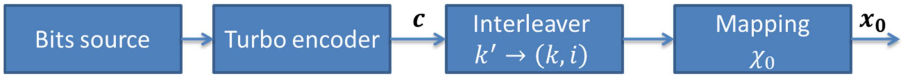

Figure 19: Mapping of bits into symbols at eNB side.

The notations beyond are used in this sub-section:

- $\boldsymbol{c}$ is the coded bit sequence,
- $c_{k'} \in \boldsymbol{c}$ is the coded bit at position k'at the input of the interleaver,
- $\boldsymbol{x}_0$ is the complex symbol sequence, symbols belong to the alphabet χ_0 of cardinal M_0,
- $x_{0,k} \in \boldsymbol{x}_0$ is the symbol at the output of mapping, where k denotes the k^{th} Resource Element (RE); notations $x_{1,k}, x_{2,k}$, χ_1 and χ_2 are used for interfering UEs.

The bit $c_{k'}$ is mapped on bit i of the symbol $x_{0,k}$. Without loss of generality the index k of the RE is dropped in the following.

At the receiver, soft decision of the bit $\mathrm{c_{k'}}$ of $\mathrm{x_0}$, also known as LLR, is given as:

$$LLR^i(c_{k'} | \boldsymbol{y}, \boldsymbol{H}_{1,0}, \boldsymbol{H_{2,0}}, \boldsymbol{W}) = \log \frac{p(c_{k'} = 1 | \boldsymbol{y}, \boldsymbol{H}_{1,0}, \boldsymbol{H_{2,0}}, \boldsymbol{W})}{p(c_{k'} = 0 | \boldsymbol{y}, \boldsymbol{H}_{1,0}, \boldsymbol{H_{2,0}}, \boldsymbol{W})} \tag{3.53}$$

where $\boldsymbol{W}$ is the matrix made of all the precoders.

The bit metric (3.54) is introduced. The log-sum approximation is used to derive the approximate value of the bit metric.

$$\Lambda_b^i(\boldsymbol{y}, c_{k'}) = \log\left(p\left(c_{k'} = b \middle| \boldsymbol{y}, \boldsymbol{H}_{1,0}, \boldsymbol{H_{2,0}}, \boldsymbol{W}\right)\right)$$

$$\Lambda_b^i(\boldsymbol{y}, c_{k'}) \approx \min_{x_0 \in \mathcal{X}_{0,b}^i,\ x_{\{1,2\}} \in \mathcal{X}_{\{1,2\}}} \left| \boldsymbol{y} - x_0(\boldsymbol{H}_{1,0}\boldsymbol{w}_{1,0} + \boldsymbol{H}_{2,0}\boldsymbol{w}_{2,0}) - \sum_{i=1}^{2} \boldsymbol{H}_{i,0}\boldsymbol{w}_{i,i}x_i \right|^2 \quad (3.54)$$

$\mathcal{X}_{0,b}^i$ denotes the subset of the signal set $x_0 \in \chi_0$ whose labels have the value $b \in \{0,1\}$ in the position i.

The bit metric for the scenario of Figure 17 can be written as in (3.55), assuming that x_1 and x_2 belong to constellations with the same energy. Some terms could have been ignored as they are independent of the minimization problem.

$$\begin{aligned} \Lambda_b^i(\boldsymbol{y}, c_{k'}) &\approx \min_{x_0 \in \mathcal{X}_{0,b}^i,\ x_{\{1,2\}} \in \mathcal{X}_{\{1,2\}}} \left\{ \left(\rho_{0,1}x_1x_0^*\right)_R + \left(\rho_{0,2}x_2x_0^*\right)_R - (\bar{y}_0^*x_0)_R - (\bar{y}_1^*x_1)_R - (\bar{y}_2^*x_2)_R \right\} \\ &\approx \min_{x_0 \in \mathcal{X}_{0,b}^i,\ x_{\{1,2\}} \in \mathcal{X}_{\{1,2\}}} \left\{ -(\bar{y}_0^*x_0)_R + \psi_{A,1}x_{1,R} + \psi_{B,1}x_{1,I} + \psi_{A,2}x_{2,R} + \psi_{B,2}x_{2,I} \right\} \end{aligned} \quad (3.55)$$

With:

- $(x)_R$ or x_R the real part of x, $(x)_I$ or x_I the imaginary part of x,
- $\rho_{0,t} = \left(\boldsymbol{H}_{1,0}\boldsymbol{w}_{1,0} + \boldsymbol{H}_{2,0}\boldsymbol{w}_{2,0}\right)^H \left(\boldsymbol{H}_{t,0}\boldsymbol{w}_{t,\mathrm{t}}\right)$, $t \in \{1,2\}$, cross correlation between channels,
- $\bar{y}_0 = \left(\boldsymbol{H}_{1,0}\boldsymbol{w}_{1,0} + \boldsymbol{H}_{2,0}\boldsymbol{w}_{2,0}\right)^H \boldsymbol{y}$, the output of a matched filter,
- $\bar{y}_t = \left(\boldsymbol{H}_{t,0}\boldsymbol{w}_{t,\mathrm{t}}\right)^H \boldsymbol{y}$, $t \in \{1,2\}$, the output of a matched filter,
- $\psi_{A,t} = \rho_{0,t,R}x_{0,R} + \rho_{0,t,I}x_{0,I} - \bar{y}_{t,R}$, $t \in \{1,2\}$,
- $\psi_{B,t} = \rho_{0,t,R}x_{0,I} - \rho_{0,t,I}x_{0,R} - \bar{y}_{t,I}$, $t \in \{1,2\}$.

The complexity of the calculation of bit metric (3.55) is $O(M_0 \times M_1 \times M_2)$. Authors in [GHA11] have nevertheless shown that this complexity can reduce to $O(M_0)$, either for x_0, x_1 and x_2 belonging to equal energy alphabets or not (this latter case is not shown here, please refer to [GHA11]). Indeed the values of $x_{t,R}$, $t \in \{1,2\}$, and $x_{t,I}$, $t \in \{1,2\}$, which minimize (3.55) need to be in the opposite directions of $\psi_{A,t}$ and $\psi_{B,t}$ respectively, thereby avoiding search on the alphabets of x_1 and x_2 and reducing two complex dimensions in the detection. The bit metric for equal energy alphabets is finally:

$$\Lambda_b^i(\boldsymbol{y}, c_{k'}) \approx \min_{x_0 \in \mathcal{X}_{0,b}^i} -\{\bar{y}_{0,R}x_{0,R} + \bar{y}_{0,I}x_{0,I} + |\psi_{A,1}||x_{1,R}| + |\psi_{B,1}||x_{1,I}| + |\psi_{A,2}||x_{2,R}| + |\psi_{B,2}||x_{2,I}|\} \quad (3.56)$$

3.2.3 Performance evaluation

Performance of receivers presented in section 3.2.2 was evaluated for the scenario of Figure 17. Robustness of receivers was also assessed for less stringent scenarios: MU-MIMO without CoMP, or MU-MIMO CoMP with only one interferer.

3.2.3.1 *Simulation tool*

Results were obtained with a complete link-level OFDM transmission chain. Main parameters of this simulator can be found in Table 1.

Table 1: Parameters of the OFDM link-level simulator.

Parameter	Value
N_T	2
N_R	2
Codebook	LTE (see below)
Channel Coding	Convolutional
Modulation	QPSK
Coding rate	½
Number of carriers	1024
Guard interval	72 samples
Number of active carriers	600
Frame length	642 μs
Channel estimation	Perfect
Channel type	SCME[1]
Interfering modulation	QPSK
Interfering coding rate	½

The LTE codebook for two transmit antennas and one layer per user is used. Precoders are labelled as shown in Table 2.

Table 2: Codebook for two transmit antennas and one layer.

Index	Precoder
0	$\frac{1}{\sqrt{2}}\begin{bmatrix}1\\1\end{bmatrix}$
1	$\frac{1}{\sqrt{2}}\begin{bmatrix}1\\-1\end{bmatrix}$
2	$\frac{1}{\sqrt{2}}\begin{bmatrix}1\\j\end{bmatrix}$
3	$\frac{1}{\sqrt{2}}\begin{bmatrix}1\\-j\end{bmatrix}$

Precoders 0 and 1 (resp. 2 and 3) are orthogonal. It must be noticed that these precoders have a coarse spatial granularity, see Figure 20. On this figure the antenna array gain is plotted. The eNB array broadside is the horizontal line passing through the point '0'.

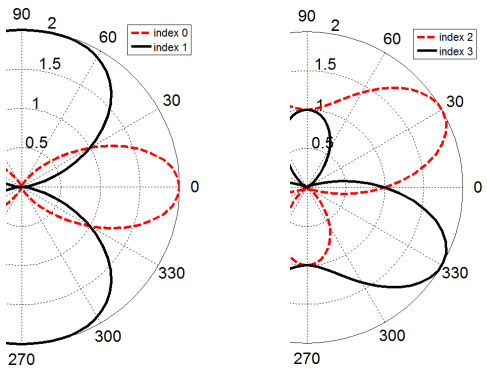

Figure 20: Beams of two antennas codebook.

[1]Spatial Channel Model Extended (SCME) [TR25.996] is a geometric and statistical MIMO channel model. The channel impulse response is computed based on stochastic distribution of clusters.

3.2.3.2 *Non interference aware receiver*

Performance of non interference aware receiver UE0 is first assessed on Figure 21 left. The scenario, MU-MIMO without CoMP, is described on Figure 21 right. Classical MRC is applied at the receiver. The curve with triangles represents the performance of the receiver without interference. Precoder #0 is applied for UE0 and precoder #1 for UE1. The position of UE0 varies from 0° (optimal position for precoder #0, see Figure 21 rigth) to 90°. Figure 21 left shows that the implementation of interference aware algorithm at the receiver is mandatory, even when the UE is ideally located w.r.t. the precoder used.

Note that the interference from UE1 only comes from data of this user and from its precoder, see equation (3.44). The channel from eNB to UE1 is not involved in the equation, the position of UE1 is therefore not simulated. However one can remark that precoder #1, used for this user, is optimal for a position of UE1 between 60° and 90°, see Figure 20.

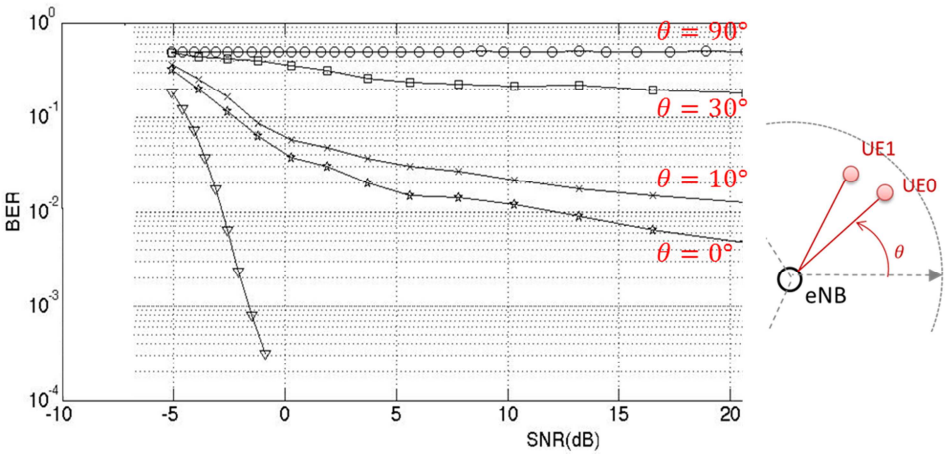

Figure 21: (left) Performance of non interference aware receiver (right) scenario.

3.2.3.3 *MU-MIMO with best precoder*

Performances of UE0 with IA-ML, MMSE-AIC and SL-MMSE algorithms are presented in Figure 22 left for the scenario of Figure 22 right. The scenario is MU-MIMO without CoMP, with UE0 located on the eNB broadside. Precoder #0 is applied for UE0 and precoder #1 for UE1. It must first be noticed that the three receivers allow for a complete rejection of the interference. Nevertheless IA-ML is by far the best receiver (SNR=7dB @ BER=10-4), followed by MMSE-AIC (SNR=17dB @ BER=10-4) and SL-MMSE (SNR=27dB @ BER=10-4).

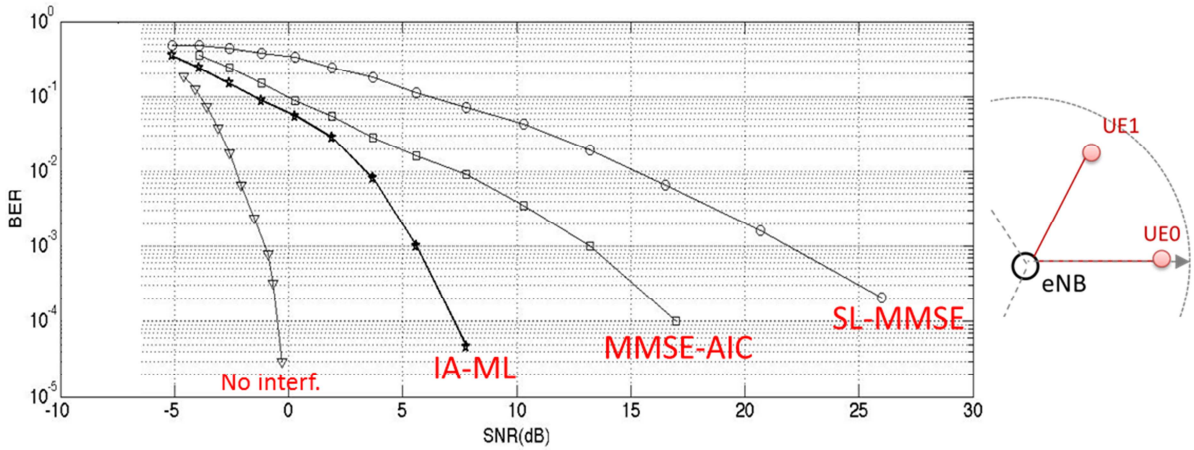

Figure 22:(left) Performance of interference aware receivers with best precoder (right) scenario.

3.2.3.4 *MU-MIMO with non-suited precoder*

Figure 23 left presents the deterioration of the performance of receivers in previous section (3.2.3.3) when UE0 is located like shown on Figure 23 right. Precoder#0 is still applied for

UE0 and precoder #1 for UE1; i.e. the precoder for UE0 is not adapted to its position. The three receivers still manage to reject all the interference, but at the cost of a much higher required SNR. Performances of MMSE-AIC strongly decrease. IA-ML remains the best receiver. It is shown to be relatively robust to a bad choice of precoder.

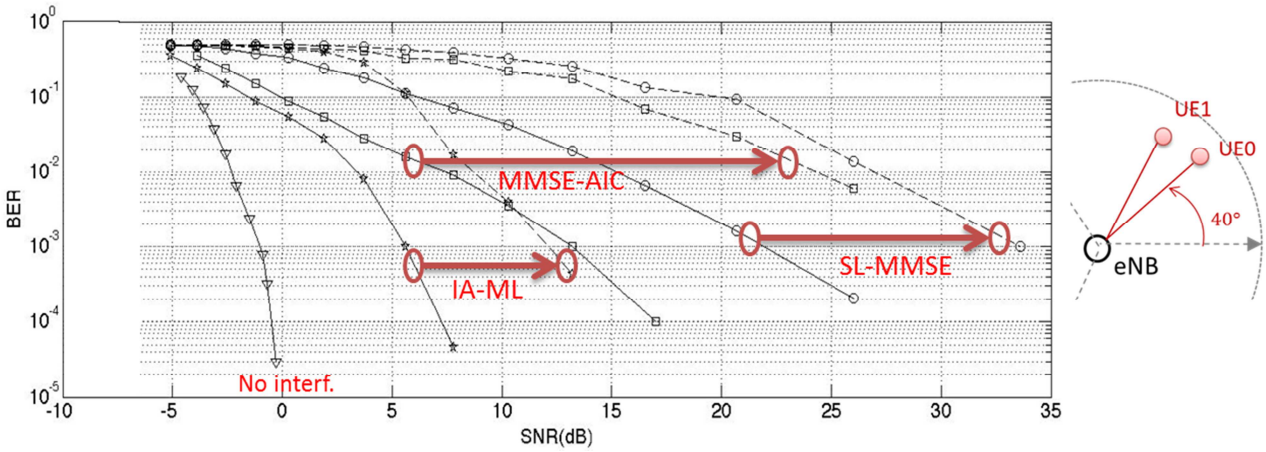

Figure 23: (left) Performance of interference aware receivers with non-suited precoder (right) scenario. Solid lines: scenario of Figure 22 right. Dashed lines: scenario of Figure 23 right.

3.2.3.5 *MU-MIMO CoMP with one interferer*

Performance of interference aware receivers are here assessed with cooperation between cells (CoMP) and compared with performance without CoMP. The two scenarios are described on Figure 24. On the left, eNB1 serves two users in MU-MIMO mode. On the right, UE0 is served in CoMP and eNB1 serves two users in MU-MIMO mode. In these scenarios, precoder #0 is used for UE0 at eNB1 and precoder #2 is used for UE0 at eNB2. Orthogonal precoder (#1) is used for UE1.

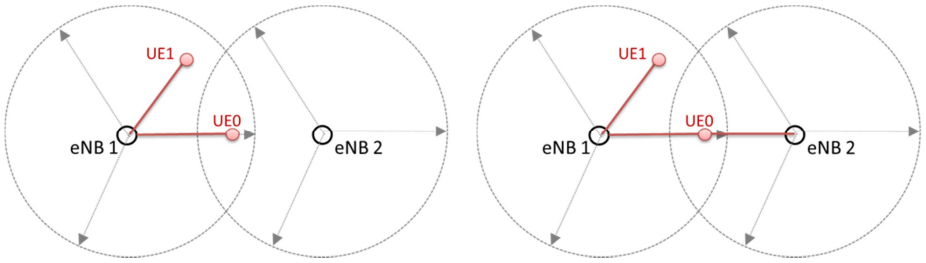

Figure 24: Scenarios of Figure 25.

On Figure 25 the BER of UE0 is plotted vs the distance eNB1-UE0. The Inter Site Distance (distance eNB1-eNB2) is 500m. The BER of IA-ML for the scenario with CoMP is null and therefore does not appear on the figure. Without cooperation the BER dramatically increases when UE0 moves away from eNB1. The best receiver in this configuration is IA-ML. Its performance is good as long as UE0 is not more than 200m away from eNB1. With CoMP, IA-ML is the only receiver that allows for a null BER at the border of the cell.

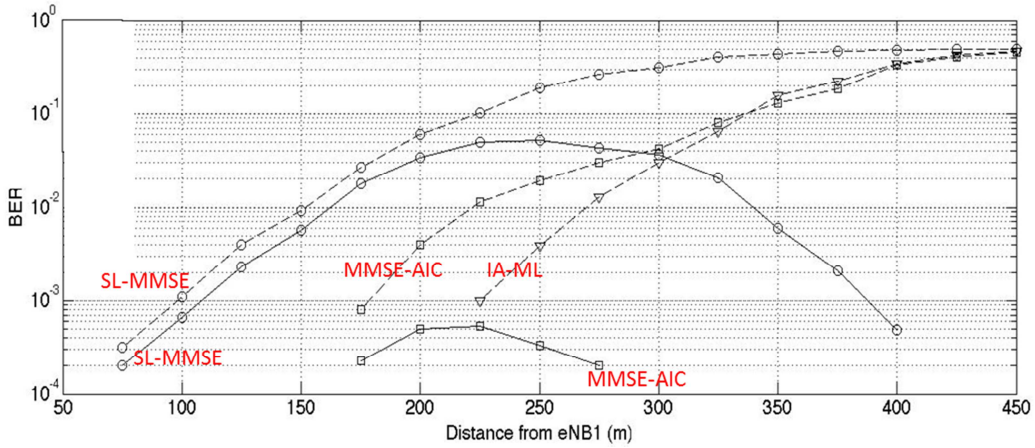

Figure 25: Dashed lines: scenario of Figure 24 left, no CoMP.Solid lines: scenario of Figure 24 right, CoMP

3.2.3.6 *MU-MIMO CoMP with two interferers*

Performance of interference aware receivers are here assessed with cooperation between cells and two interferers. They are compared to the scenario with one interferer of Figure 24 right. The two scenarios are described on Figure 26. On the right, UE0 is served in CoMP and both eNB1 and eNB2 serve two users in MU-MIMO mode. In these scenarios, precoder #0 is used for UE0 at eNB1 and precoder #2 is used for UE0 at eNB2. Orthogonal precoders (resp. #1 and #3) are used for UE1 and UE2.

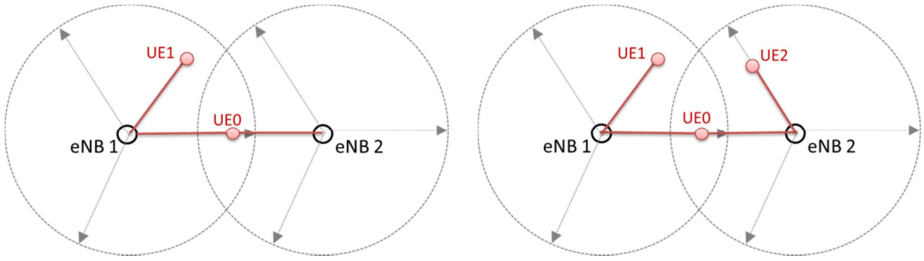

Figure 26: Scenarios of Figure 27.

On Figure 27 the BER of UE0 is plotted vs the distance eNB1-UE0. The Inter Site Distance (distance eNB1-eNB2) is 500m. The BER of IA-ML for the scenario with one interferer is null and therefore does not appear on the figure. It must be noticed that when two interferers are present, none of the receivers allow for a null BER at the edge of the cell.

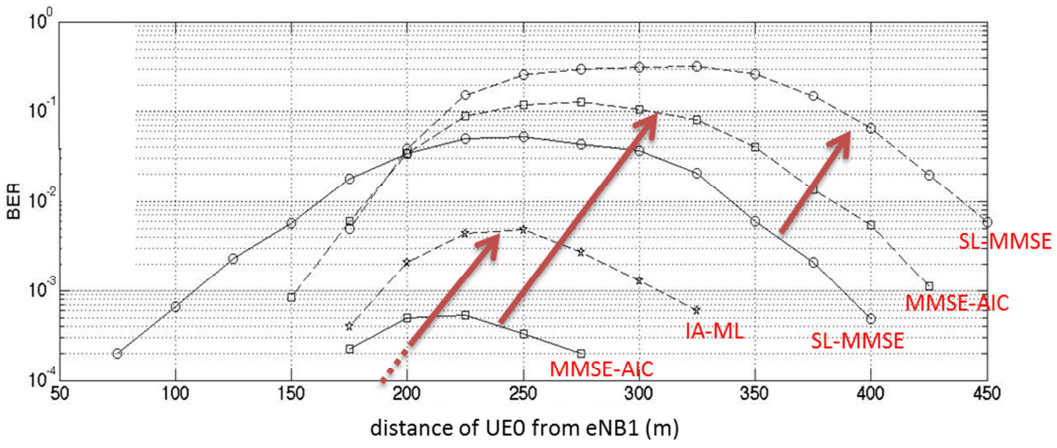

Figure 27: Solid lines: scenario of Figure 26 left, one interferer. Dashed lines: scenario of Figure 26 right, two interferers

3.2.4 Conclusion

This study aimed at assessing the performances of interference aware receivers for MU-MIMO CoMP with LTE precoders. As a first step, perfect knowledge of channel of interfering precoders was supposed at the receiver.

It was firstly shown that implementing interference aware algorithms at the receiver, in MU-MIMO mode, is mandatory. The level of interference caused by the poor resolution of precoders indeed creates a high BER floor.

In MU-MIMO mode, without CoMP, interference aware receivers were secondly proved to be able to reject all interference when the SNR is high.

In MU-MIMO CoMP mode, with only one interferer, IA-ML algorithm was shown to be the only one among the implemented algorithms to cancel all interference at the border of the cell.

Finally, the scheme of Figure 17, with three UEs and thus two interferers, was demonstrated to generate too much interference to perfectly demodulate the signal of UE0 at the cell edge.

Further work will consist in introducing more realistic assumptions in the scenario, i.e. real channel estimation or error on the interfering constellation. A scenario with four transmit antennas will also be considered.

3.3 Cross-layer Performance Evaluation of CoMP

3.3.1 Introduction

Mobility is an essential and important mechanism in wireless communications. This mechanism has a significant impact on the performance of the wireless systems. For mobile networks, the variation of the fading experienced by the mobile user depends on the speed of the device. Moreover the mean radio conditions mainly determined by the path loss attenuation due to distance are no more constant over the service period. Thus a user can move from 'BAD' to 'GOOD' conditions and vice versa. The larger the instantaneous fluctuations, the larger the diversity gain will be.

3.3.2 Queuing Model

In order to study the impact of mobility on users' data rates, we have introduced, as a first step, new models including mobility mechanisms in order to obtain quantitative performance results. We have evaluated different scheduling strategies and we have shown that mobility increases the capacity of the system regardless of the resource sharing policy. We studied the impact of mobility, without considering fading. However, in a real network environment, the signal received by a user is affected by fading due to multi path propagation. Thus, we present here the impact of fading. The performance evaluation is also done through system level simulations, in order to validate the proposed analytical models.

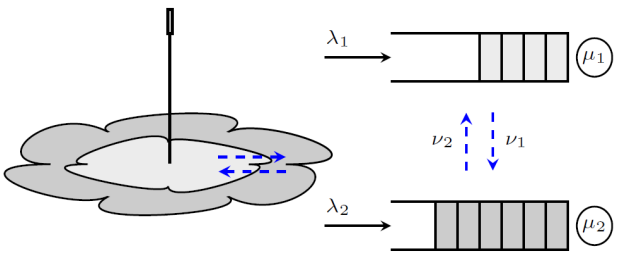

Figure 28: Queuing Model including mobility.

The two studied scheduling disciplines are:

Round Robin: where resources are fairly shared between users regardless of their channel conditions. This method tries to dynamically allocate resources between the two types of

users based on the number of users in each class without taking into account channel conditions.

Max C/I: is an opportunistic scheduling strategy that prioritizes users with better channel conditions, so that users in the center are scheduled first and allocated all resources when present in the network, where cell edge users are served only when first queue empties, and there are no users with better conditions waiting for service.

3.3.2.1 *Impact of fading*

In the previous work, we ignored the fact that in a real network environment, the signal received by a user is affected by fading that may be due to multi path propagation, with the aim of exploring the impact of mobility. Indeed, fading could be beneficial if an opportunistic scheduling is done even for static users. We denote by $G(n)$ the scheduling gain brought by an opportunistic scheduler compared to a blind round robin scheduler, when users have fading statistics.

For Rayleigh fading, users SINR $S_{1,2,\dots n}$ are exponentially distributed.

It was shown that for small values of SINR where the variation of data rate is considered linear with respect to this latter:

$$G(n) = E[max(S_1, S_2, \dots S_n)] = 1 + 1/2 + \cdots + 1/n \quad (3.57)$$

n is the number of users to be scheduled.

But since the gain brought by fading to SINR doesn't correspond exactly to the gain of data rate, we define $G'(n)$ the gain of data rate based on Shannon's channel capacity:

$$G'(n) = \frac{E[log_2(1 + Y_n)]}{E[log_2(1 + Y_1)]} \quad (3.58)$$

where $Y_i = max(S_1, S_2, \dots S_i)$. Thus, $Y_1 = max(S_1)$ and $Y_n = max(S_1, S_2, \dots S_n)$.

Then the instantaneous maximum service rate in each queue when adopting a MaxC/I scheduler can be written as:

$$\mu'_i(t) = \mu_i . G'_i(x_i(t)) \quad \text{i=1,2} \quad (3.59)$$

Where μ_1 and μ_2 are mean service rates in cell-center and cell-edge respectively, as shown in Figure 28.

$x_i(t)$ is the instantaneous number of users in queue i $(= 1,2)$.

Figure 29 shows the variation of scheduling SINR gain $G(n)$ and scheduling rate gain $G'(n)$ as a function of the number n of users sharing cell resources.

3.3.2.2 *Numerical Results and analysis*

Numerical results shown in the following figures are obtained for the same particular scenario of the previous section. However we take into account the effect of fading in a system implementing a MaxC/I scheduler.

Average mean user throughputs of both scheduling methods are shown in Figure 30. Compared to previous results, MaxC/I shows a considerable improvement in throughput due to fading in the static case (ν=0). Then an additional gain is brought by mobility when ν=0.1. Note that ν represents the mean speed at wich a user moves normalized over the mean distance that should be traveled to change region.

Moreover a MaxC/I scheduler is better in terms of throughput for cell-center users as shown in Figure 31 as well as for static and mobile cell-edge users as Figure 32 shows. That means that it is better for all users to do an opportunistic scheduling than a fair scheduling in a real network with fading.

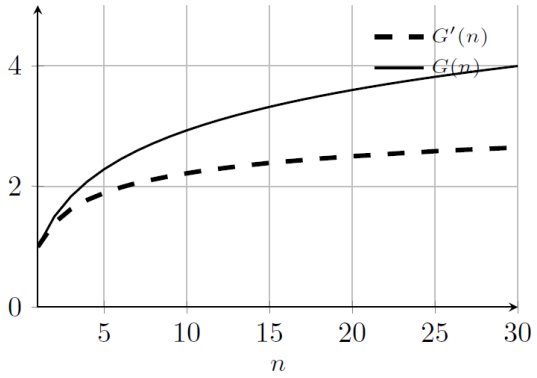

Figure 29: Scheduling SINR gain G(n) and rate gain G'(n).

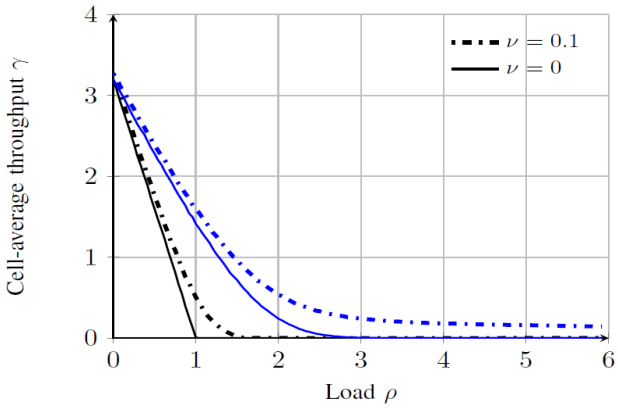

Figure 30: Cell-average throughput (in σ *bps*) for RR (black) &MaxC/I (blue).

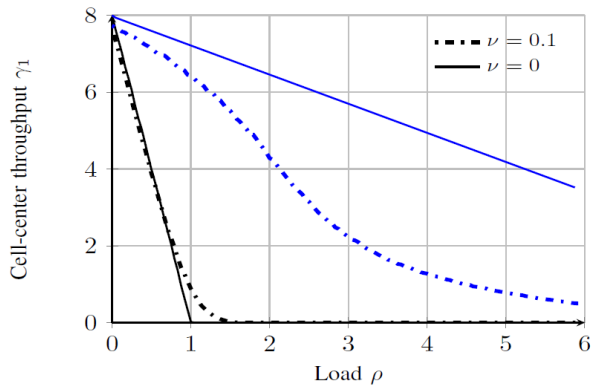

Figure 31: Mean cell-center user throughput (in σ *bps*) for RR (black) &MaxC/I (blue).

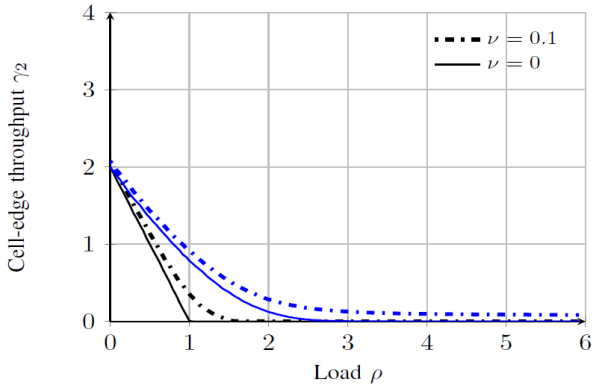

Figure 32: Mean cell-edge user throughput (in σ *bps*) for RR (black) &MaxC/I (blue).

3.3.3 System simulation

3.3.3.1 *Simulator description*

In the previous section we focused on analytical performance evaluation based on queuing theory. We proposed a Markovian model that takes into account mobility of users in a cellular network. In this section we aim to validate this model by system level simulations. Thereby simulations are done for 21 cells constituting 7 tri-sectoral sites as shown in Figure 33. Spatially correlated shadowing maps for different sites are generated each 3s. Those maps are also correlated in time. Furthermore, 21*(4 spatially correlated fading complex values) are generated for each user each TTI or 1ms. The characteristics of the Simulator are shown in the following table. Traffic model is elastic and arrival process is Poisson with constant mean arrival rate per eNodeB. Requested service is file download. File lengths are generated from an exponential distribution with mean σ=4dB. Scheduling decisions are taken in each eNodeB each TTI. In order to evaluate the proposed model, the two previous schedulers are implemented. The blind round robin scheduler enables to serve a different user each TTI, regardless of his channel condition. The MaxC/I scheduler chooses each TTI the user with highest instantaneous SINR. We study two scenarios, in the first one all users are static users. In the second scenario, all users are moving at a speed of 300 km/h. We simulate 10 minutes and we calculate for each scenario the average of all users throughputs weighted by sojourn times.

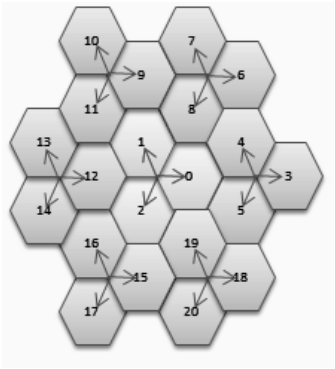

Figure 33: Map.

Table 3: Simulator characteristics.

Network topology	Macro cells only
Environment	Urban
Context	outdoor
Inter-site distance	500 m
Resolution	5 m
PathLoss	ITU Model
shadowing std	4 dB
shadowing cross correlation (between sites)	0.5
shadowing spatial correlation	$e^{\frac{-\delta d}{d_{corr}}}$
shadowing correlation distance	d_{corr}: 30 m
Radio access technology	LTE
Number of tx/rx antennas	MIMO (2x2)
number of streams	1
Receiver	MRC
Codebook	3GPP
carrier frequency	2 GHz
Bandwidth	10 MHz

3.3.3.2 ***Results and analysis***

Figure 34 shows the variation of mean user throughput in b/s/Hz as a function of the arrival rate per eNodeB when users are static as well as when they are moving (v=300 km/h).

Results are very close to those obtained by queuing theory analysis. Compared to Figure 30, curves profiles are almost the same.

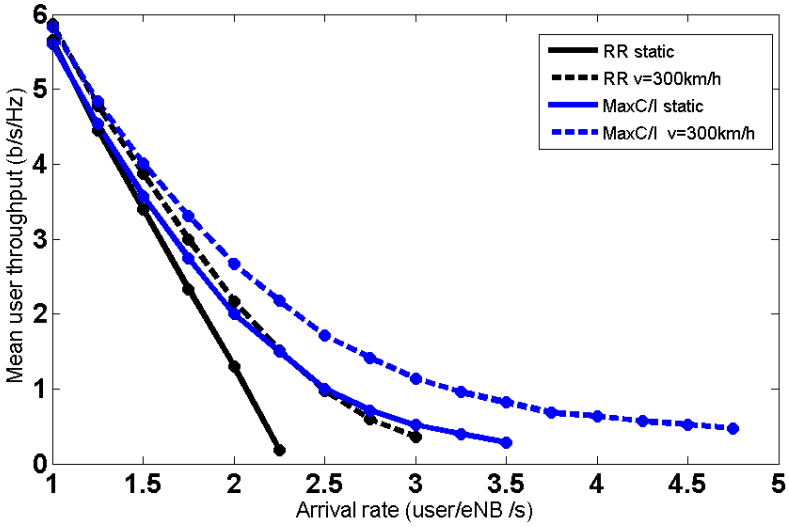

Figure 34: Average mean user throughput.

3.3.4 Conclusion

In this work, we studied the impact of mobility on a cellular system through flow level analysis. We have proposed a model for mobility, based on Markovian queuing models. Then we tested the reliability of the proposed analytical model through system level simulations. Unlike fast fading, we have shown that mobility tends to increase the capacity regardless of the scheduling policy (Note that these simulations don't take into account the feedback delay).

However the performance improvement when adopting an opportunistic scheduling is more significant. Indeed prioritizing users with better channel conditions, gives the opportunity to mobile cell-edge users to get better conditions. But this is not the case for a static cell-edge user whose mean channel conditions remain constant over the service period. Thus a more advanced scheduling strategy that exploits the information of mobility of users could be an interesting direction for further research.

3.4 Transmitter-side Solutions to Suppress or Avoid Interference with Advanced MIMO Schemes

3.4.1 Objectives and model description

3.4.1.1 *Objectives*

The main objective is to assess the performance of advanced MIMO schemes having interference cancellation capability. MIMO based transmission allows to provide a BER gain thanks to the presence of antenna diversity, in addition to a possible data throughput increase. In a multi-user context, it is also compulsory to have an interference cancellation capability.

In this study, we focus on linear dispersive (LD) codes [HEA02], [HAS02], which are very promising MIMO codes. They provide a good tradeoff between spatial multiplexing gain and a gain in spatial diversity, and can also provide a temporal diversity gain. The linearity of the coding allows to use medium complex processing at the receiver (SIC, or ML implemented with sphere decoder). Such codes are designed for any number of transmit and/or receive antennas.

The receivers associated to LD codes at transmission are widely linear (see paragraph below for definition) whatever the constellation is.

In this first contribution, an analysis on state-of-the-art processing is carried out and performance evaluation is presented. Further contribution will focus on more complex LD codes at transmission.

3.4.1.2 *Model description*

We assume that the transmitters have 2 antennas and implement the Alamouti scheme, see reference [ALA98], according the coding matrix **S** defined at time n by:

$$\mathbf{S_n} = \begin{pmatrix} -\mathrm{s}_{2(2n)}^{*} & \mathrm{s}_{1(2n-1)} \\ \mathrm{s}_{1(2n)}^{*} & \mathrm{s}_{2(2n-1)} \end{pmatrix} \tag{3.60}$$

The transmitted symbols s_i are taken either from a real valued constellation or from a complex constellation.

The receiver is equipped with N antennas. T is the symbol duration.
Let $\mathbf{x}_1(n)$ be the (N,1) received vector sampled at time (2n-1)T and $\mathbf{x}_2(n)$ the received vector sampled at time (2n)T.

$$\begin{aligned} \mathbf{x_1}(n) &= \mu \boldsymbol{h_1} \mathrm{s}_1(2n-1) + \mu \boldsymbol{h_2} \mathrm{s}_2(2n-1) + \boldsymbol{b}(2n-1) \\ \mathbf{x_2}(n) &= -\mu \boldsymbol{h_1} s_2^{*}(2n) + \mu \boldsymbol{h_2} \mathrm{s}_1^{*}(2n) + \boldsymbol{b}(2n) \end{aligned} \tag{3.61}$$

where $\boldsymbol{h_1}$ (resp. $\boldsymbol{h_2}$) is the channel vector of dimension (N,1) between the first (resp. second) transmit antenna and the receiver. Channel vectors $\boldsymbol{h_i}$, i=1,2 are normalized such that $E\left[\mathbf{h}_i^{\boldsymbol{H}} \boldsymbol{h_i}\right] = N$. $\boldsymbol{b}$ is the noise vector at reception.
We assume that both transmit antennas transmit the symbols at the same power level $\mu = \sqrt{\rho/2}$, where ρ is the SNR at reception.

Let us note x, $\bar{\mathrm{x}}$, $\tilde{\mathrm{x}}$ the following vectors:

$$\mathbf{x} = \begin{bmatrix} \mathbf{x_1} \\ \mathbf{x_2} \end{bmatrix}, \bar{\mathbf{x}} = \begin{bmatrix} \mathbf{x_1} \\ \mathbf{x_2^{*}} \end{bmatrix}, \tilde{\mathbf{x}} = \begin{bmatrix} \mathbf{x} \\ \mathbf{x}^{*} \end{bmatrix} \tag{3.62}$$

We consider the presence of a synchronous intra network interfering user in addition to the useful user. Rayleigh channel, with narrow band waveform and flat fading are considered.

3.4.2 MMSE interference cancellation with Alamouti Code

In this section we analyse state-of-the-art interference cancellation processing when Alamouti code is used at transmission.

3.4.2.1 *Alamouti MMSE*

A MMSE receiver can be implemented for the reception of the Alamouti useful signal in presence of synchronous Alamouti intra network interferers, see reference [NAG98]. The received signal is filtered according to a MMSE criterion. A ML detection is then implemented. The detected symbols are written as follows:

$$\begin{aligned} \hat{s}_{1,mmse}(n) &= argmin_{\hat{s}_1}\left\{\left\| \boldsymbol{W_{1mmse}^{H}} \bar{\mathbf{x}}(n) - \hat{s}_1 \right\|^2\right\} \\ \hat{s}_{2,mmse}(n) &= argmin_{\hat{s}_2}\left\{\left\| \boldsymbol{W_{2mmse}^{H}} \bar{\mathbf{x}}(n) - \hat{s}_2 \right\|^2\right\} \end{aligned} \tag{3.63}$$

Where

- $\boldsymbol{W_{1mmse} = R_{\bar{x}}^{-1} g_1}$ and $\boldsymbol{W_{2mmse} = R_{\bar{x}}^{-1} g_2}$
- $\boldsymbol{R_{\bar{x}}} = E[\overline{\boldsymbol{x}}\overline{\boldsymbol{x}}^{\boldsymbol{H}}]$, of dimension (2N,2N)
- $\boldsymbol{g_1} = \begin{bmatrix} \boldsymbol{h_1} \\ \boldsymbol{h_2^*} \end{bmatrix}$ and $\boldsymbol{g_2} = \begin{bmatrix} \boldsymbol{h_2} \\ -\boldsymbol{h_1^*} \end{bmatrix}$, of dimension (2N,1)

Such an interference cancellation processing can completely suppress the signal from N-1 internal interferers, hence with N=2 receive antennas, the receiver can suppress one interferer. A diversity gain is provided by the Alamouti code and the decoding processing has a low complexity.

3.4.2.2 *Alamouti WL-MMSE*

A new MMSE receiver based on a widely linear processing has been proposed in [CHE11]. The receiver processes $\tilde{\mathbf{x}}$ instead of $\bar{\mathbf{x}}$, allowing to take into account all the second order covariance matrices of the received signal.
This WL-MMSE Alamouti receiver can then process 2N-1 internal interferences compared to N-1 with the previous MMSE Alamouti receiver, hence a SAIC capability, i.e. the receiver can suppress one internal interferer with only N=1 receive antenna. The detected symbols are written as follows:

$$\begin{aligned} \hat{s}_{1,WLmmse}(n) &= argmin_{\hat{s}_1}\left\{\left\|\boldsymbol{W_{1WLmmse}^H}\tilde{\mathbf{x}}(n) - \hat{s}_1\right\|^2\right\} \\ \hat{s}_{2,WLmmse}(n) &= argmin_{\hat{s}_2}\left\{\left\|\boldsymbol{W_{2WLmmse}^H}\tilde{\mathbf{x}}(n) - \hat{s}_2\right\|^2\right\} \end{aligned} \quad (3.64)$$

Where

- $\boldsymbol{W_{1WLmmse} = R_{\tilde{x}}^{-1} f_1}$ and $\boldsymbol{W_{2WLmmse} = R_{\tilde{x}}^{-1} f_2}$
- $\boldsymbol{R_{\tilde{x}}} = E[\tilde{\boldsymbol{x}}\tilde{\boldsymbol{x}}^{\boldsymbol{H}}]$, of dimension (4N,4N)
- $\boldsymbol{f_1} = \begin{bmatrix} \boldsymbol{h_1} \\ \boldsymbol{h_2} \\ \boldsymbol{h_1^*} \\ \boldsymbol{h_2^*} \end{bmatrix}$ and $\boldsymbol{f_2} = \begin{bmatrix} \boldsymbol{h_2} \\ -\boldsymbol{h_1} \\ \boldsymbol{h_2^*} \\ -\boldsymbol{h_1^*} \end{bmatrix}$, of dimension (4N,1)
- $\boldsymbol{R_{\tilde{x}}} = \begin{pmatrix} R_x & C_x \\ C_x^* & R_x^* \end{pmatrix}$ with $C_x = E[\boldsymbol{x}\boldsymbol{x}^{\boldsymbol{T}}]$ and $R_x = E[\boldsymbol{x}\boldsymbol{x}^{\boldsymbol{H}}]$

As exposed in [AGH10], we have the following expression:

$$C_x = \begin{pmatrix} C_1 & C_{12} \\ C_{12} & C_2 \end{pmatrix} = \begin{pmatrix} h_1^2\gamma_{x1}^2 - h_2^2\gamma_{x2}^2 & h_1h_2(\sigma_{x1}^2 - \sigma_{x2}^2) \\ h_1h_2(\sigma_{x1}^2 - \sigma_{x2}^2) & h_1^2(\gamma_{x1}^2)^* + h_2^2(\gamma_{x2}^2)^* \end{pmatrix} \quad (3.65)$$

Where σ_{si}^2 and γ_{si}^2 are the variance and pseudo variance of symbols s_i.

3.4.2.3 *Comparison of Alamouti-MMSE and Alamouti-WL MMSE*

Second degrees statistics of the received signal are R_1, R_2, C_{12}, C_1, C_2, R_{12}. Hence the MMSE and WL-MMSE differ as:

- $\boldsymbol{R}_{\bar{x}} = E[\bar{\boldsymbol{x}}\bar{\boldsymbol{x}}^{\boldsymbol{H}}]$ has components R_1, R_2, C_{12}
- $\boldsymbol{R}_{\tilde{x}} = E[\tilde{\boldsymbol{x}}\tilde{\boldsymbol{x}}^{\boldsymbol{H}}]$ has components R_1, R_2, C_{12}& C_1, C_2, R_{12}

When using the Alamouti code, we can then find the configurations where it is better to use the widely linear receiver than the MMSE receiver. We have WL-MMSE better than MMSE receiver when:

$$\sigma_{s1}{}^2 = \sigma_{s2}{}^2$$

and

$$\gamma_{s1}{}^2 = \gamma_{s2}{}^2 \neq 0 \; \epsilon \; \mathcal{H}$$

- With ASK modulations (non circular Second-Order [SO] signal)
  $\sigma_{si}{}^2 = \gamma_{si}{}^2 = \alpha \neq 0 \Rightarrow C_x$ has non zeros components: C_1 & C_2

  WL-MMSE is better than MMSE receiver.
- With MPSK (M>2) modulations
  $\gamma_{si}{}^2 = 0 \Rightarrow Cx=0$

  WL-MMSE is equivalent to the MMSE receiver.

3.4.2.4 *Simulation results*

Figure 35 and Figure 36 present simulation results for N=1 and N=2 without interferer and with one internal interferer. MMSE and WL-MMSE Alamouti processing are compared. Rayleigh propagation channels are simulated between the user (resp. interferer) and the receiver. BPSK constellation is used. BER are assessed on 10^6 channel and noise realisations. "PWL" denotes partially widely linear processing and "FWL" denotes fully widely linear processing.

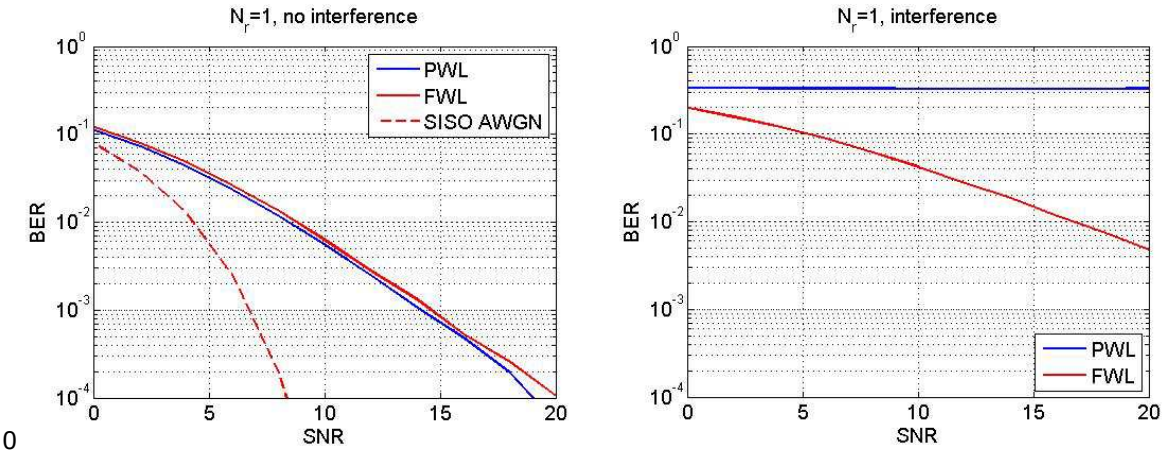

0

Figure 35: MMSE and WL-MMSE without and with interference, N=1.

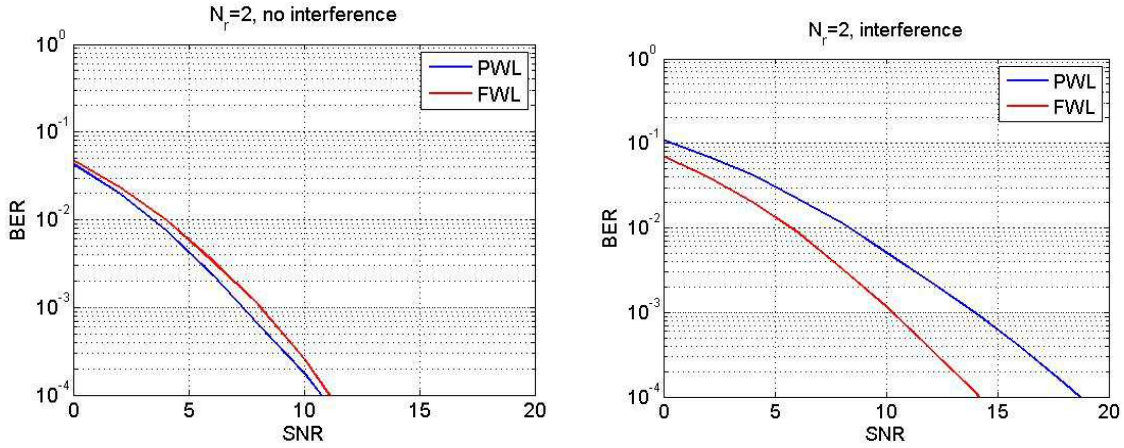

Figure 36: MMSE and WL-MMSE without and with interference, N=2.

Figure 37 presents BER results when useful signal is SO Circular (here a QPSK) and is corrupted by an SO non circular external interference (BPSK).

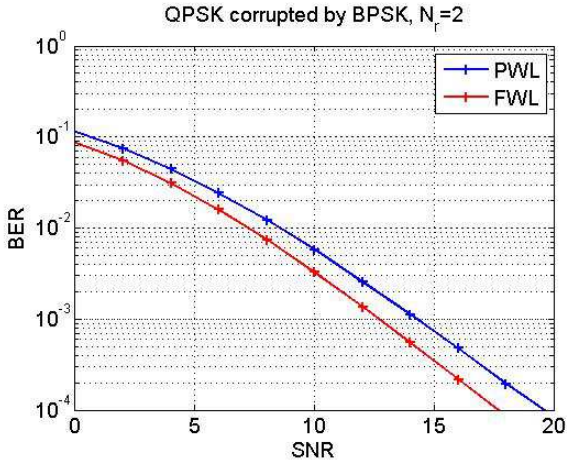

Figure 37: MMSE and WL-MMSE with external interference, N=2.

We conclude from this first analysis that the widely linear processing improves the BER performance compared to the Alamouti-MMSE receiver.

When the useful signal is SO non circular as BPSK, the WL receiver improves the jamming rejection when the number of receive antennas N is greater than 1. It also provides a SAIC capability when N=1, e.g. it can suppress one SO non circular interference with only one receive antenna at reception.

When the useful signals are higher order constellation, the WL-MMSE processing provides performance improvement when there are SO non circular interferers, such as BPSK, ASK, OQPSK, OQAM, GMSK, especially when N>1.

3.4.3 **Further works**

As the use of Alamouti code and MPSK (M>2) at transmission will always lead to null second order statistics, one of the objective is to look for more complex linear dispersive codes which woul lead to better performance.

Further work will thus follow up the study on Linear dispersive codes and widely linear receivers, and more especially when the number of transmit antennas is greater than 2. An analysis of the impact of WL-MMSE processing compared to the MMSE receiver will be carried out, as well as performance evaluation.

4 IMPACT OF BEAMFORMING IN A LARGE-SCALE REAL ENVIRONMENT

In this section we go further in the analysis of the macro-only network initiated in deliverable D3.4 [D3.4], by evaluating the impact of beamforming. We consider here the LTE Transmission Mode (TM6) which is denoted as "Closed loop spatial multiplexing using a single transmission layer". This is a special type of closed loop spatial multiplexing (TM4) in which a single layer is used [RS11]. The precoding matrices in the two antennas case are given in Table 2. The phase shift between antenna ports results in a beamforming effect as shown by the equivalent relative gain in Figure 20. A 3 dB gain can be achieved in the optimal direction of each beamforming pattern thanks to in-phase signal reconstruction in the far field region. Sixteen precoding matrices exist in the four antennas case, eight of them achieving a 6 dB gain in the optimal direction.

During active communication, the UE estimates the channel and feeds back the most suitable precoding matrix index to the eNB. When data is transmitted to the UE, the eNB sends the precoded signal via all antenna ports, and the beamforming effect has the following consequences:

- The signal in the beamforming pattern is increased
  - ➔ The signal towards the UE is increased.
  - ➔ The interference to other cells is increased in that direction.
- The signal out of the beamforming pattern is decreased
  - ➔ The interference to other cells is decreased in these directions.

The impact on the SINR, and then on link performance, is thus not straightforward. It depends on whether the interference increase is higher or lower than the useful signal increase at the UE. The following study thus evaluates the impact of beamforming in the DL at the network level.

The network description and real environment are described in [D3.4]. We still assume a single antenna at the UE side, but one, two or four co-polarized antennas at the eNB side with half-wavelength separation. Path-loss and MIMO channel properties from each eNB are computed with a highly efficient ray-based propagation model [COR09]. In addition to the path-loss calculation and best-server map processing, the UE channel estimation and codebook index selection is simulated, assuming it is the one maximizing the received power. In the same way as the best-server map representing cell-selection was established (see [D3.4]), a best-code map representing code selection is available within each cell. Figure 38 shows the one obtained for the first sector of the central site of the scenario under study. This best-code map is not necessarily correlated to the beamforming pattern, especially with low eNBs in dense urban areas, where multiple paths and canyoning effect make the strongest propagation paths different from the direct one.

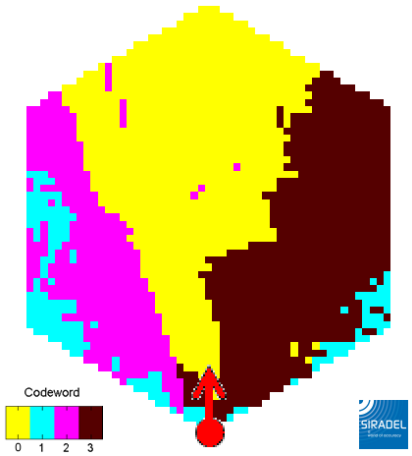

Figure 38: Best-code map for two antennas.

This best-code map is the basis of user traffic repartition: the spatial traffic distribution is assumed to be uniform, thus it is proportionnaly dispatched according to the code cover ratio within each cell. For instance, if code 1 is selected by 30% of the UEs in the cell, then 30% of the traffic is transmitted with code 1. The interference model introduced in D3.4 is then refined in (4.66):

$$I = \sum_{i \neq j} \sum_{c} EPRE_i . TL_i . PL_i . CC_{i,c} . W_c . H_i \qquad (4.66)$$

where:

- i is the index of the interfering cell,
- j is the index of the serving cell,
- c is the code index, ranging from 1 to 4 in the two antennas case,
- $EPRE_i$ is the Energy Per Resource Element of interfering cell i, in W,
- TL_i is the traffic load of interfering cell i,
- PL_i is the path-loss between interfering eNB i and the UE, including antenna radiation gain,
- $CC_{i,c}$ is the cover ratio of code index c within interfering cell i,
- W_c is the index c precoding matrix,
- H_i is the channel matrix between interfering eNB i and the UE.

Note that precoding matrices are normalized, thus the total transmit power remains the same whatever the number of antennas of the eNB. This makes possible a fair comparison with the single antenna case of D3.4. On one hand, the beamforming effect of the precoding matrix W_c makes the interference level increase in the direction favoured by the code c. On the other hand, the dispatching of the traffic on different codes makes the interference level decrease in average by a factor equal to the code cover ratio $CC_{i,c}$. Finally, the SINR is given by:

$$SINR = \frac{EPRE_j . PL_j . W_{UE} . H_j}{\sum_{i \neq j} \sum_{c} EPRE_i . TL_i . PL_i . CC_{i,c} . W_c . H_i + N} \qquad (4.67)$$

where:

- $EPRE_j$ is the Energy Per Resource Element of serving cell j, in W,
- PL_j is the path-loss between serving eNB j and the UE, including antenna radiation gain,
- W_{UE} is the precoding matrix selected by the UE,
- H_j is the channel matrix between serving eNB j and the UE,
- N is the background noise at the UE in W.

The impact of beamforming on the SINR is illustrated by the CDF of Figure 39 where a 50% traffic load is assumed for all cells. We observe a positive impact, with a 2.4 dB gain in average for the two antennas case, and 5 dB for the four antennas case. In only few locations, the beamforming makes the interference level increase more than the useful signal, resulting in a lower SINR. On the other hand, maximum gains are of 5.2 dB and 9.9 dB for the two and four antennas cases respectively.

Finally, the LTE channel capacity is determined from a link-to-system mapping table [MEH09], which maps the SINR to the achievable modulation and coding rate. Figure 40 shows the CDF of the mean user peak throughput, considering a typical 10 MHz bandwidth. It is increased of

4.1 Mbps and 9.2 Mbps in average for the two and four antennas cases respectively. The mean user peak throughput of cell-edge users (5%-ile) is 3.5, 5 and 8 Mbps for the one, two and four antennas cases respectively.

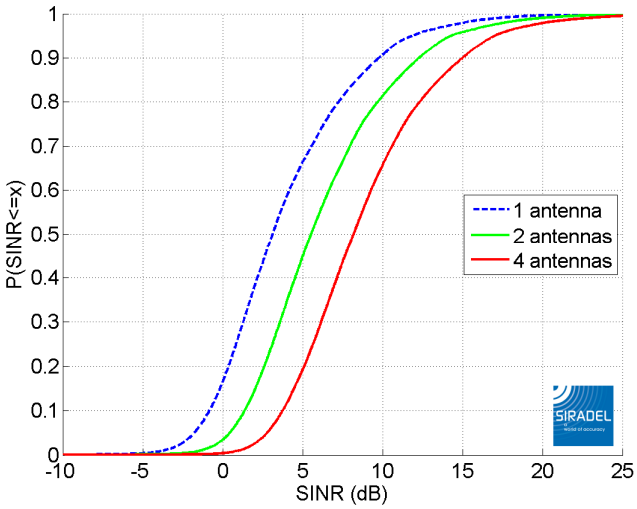

Figure 39: CDF of the SINR with two and four antennas beamforming, compared to single transmit antenna.

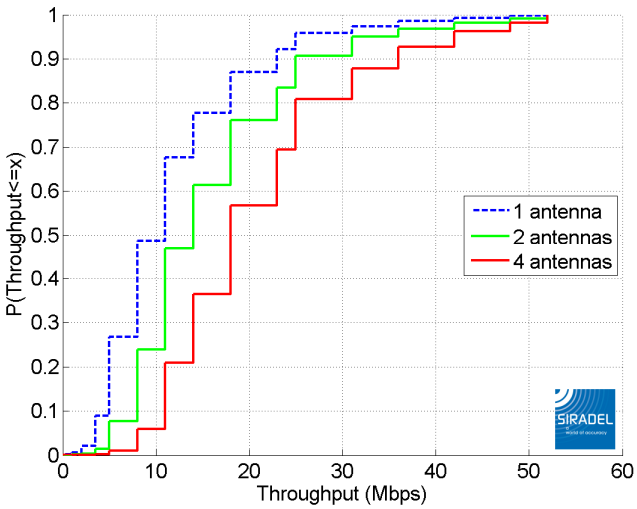

Figure 40: CDF of the mean user peak throughput with 2 and 4 antennas beamforming, compared to single transmit antenna.

These results impel to go further in the modeling approach in order to perform a deeper analysis of the beamforming impact and derive more realistic results. In this study SINR calculation actually assumes no interference mitigation mechanisms and fixed traffic loads. This simple approach does not take into account the impact of the potential decrease of interferences achieved thanks to the higher number of emitting antennas. Some perspectives for a next deliverable are thus to add some Inter-Cell Interference Coordination (ICIC) mechanisms and enhanced ICIC (eICIC) in the simulation process, and evaluate the impact on traffic loads and network energy consumption. A further evaluation could be to introduce a Coordinated Scheduling/Beamforming (CS/CB) multi-point cooperation scheme, which would optimize the use of the codes to minimize interferences.

5 CONCLUSION

This document presents first performance evaluations of innovative concepts at transmitter-side to suppress or avoid interference with CoMP and advanced MIMO schemes.

A focus is first done on CSIT, which represents an issue when multiplying the number of cooperative base stations. Feedback design studies propose solutions to exploit CSIT inaccuracies for secrecy purpose, or adapt it to the CoMP context in order to find the best feedback quantization to minimize the rate loss.

Several innovative concepts are then evaluated to jointly optimize fairness and network efficiency. Exploring different strategies that are advanced scheduling, Multi-User MIMO, mobility management or use of linear dispersive spatial temporal codes, significant gains are obtained both in average and cell-edge throughput.

Finally, the impact of beamforming is assessed in a large-scale real environment and illustrates the gain obtained in a realistic scenario.

Taking into account the drawbacks of CoMP which are the loss of resources and the backhaul overhead, these studies deliver solutions where the trade-off between fairness and network efficiency is optimized while providing gains for all users.

Next deliverable D3.6 "Performance assessments of the most promising Multi-point transmission and reception techniques" will provide the performance assessment of the most promising innovations described in this document.

REFERENCES

[AGH10] A.Aghaei, K.Plataniotis, S.Pasupathy, "Widely Linear MMSE Receivers for Linear Dispersion Space-Time Block-Codes", IEEE Trans. on Wireless Commun., volume 9, number 1, pp.8--13, Jan 2010.

[ALA98] S.Alamouti, "A Simple Transmit diversity technique for wireless communications", IEEE J. Select. Areas Commun., vol. 16, no. 8, pp. 1451-1458, Oct. 1998.

[BAI11] Zijan Bai, Biljana Basdic, Stanislaus Iwelski, Tobias Scholand, Rajarajan Balraj, Guido Bruck and Peter Jung, "On the equivalence of MMSE and IRC Receiver in MU-MIMO Systems," *IEEE Communications letter*, vol 15, N0. 12, December 2011.

[CHE11] P.Chevalier, F.Dupuy, "Widely Linear Alamouti Receiver for the reception of real-valued constellations corrupted by interferences – The Alamouti-SAIC-MAIC Concept", IEEE 2011.

[CJK10] G. Caire, N. Jindal, M. Kobayashi, N. Ravindran, "Multiuser MIMO achievable rate with downlink training and channel state feedback", IEEE Trans. Information Theory, Vol. 56, No. 6, pp. 2845-2866, Jun. 2010.

[COR09] Y. Corre and Y. Lostanlen, "Three-dimensional urban EM wave propagation model for radio network planning and optimization over large areas", IEEE Transactions on Vehicular Technology, vol. 58, no. 7, pp. 3112-3123, Sept. 2009.

[CPDF14] L. Czap, V. M. Prabhakaran, S. Diggavi, and C. Fragouli, "Secret Communication over Broadcast Channels with State-Feedback", preprint on arXiv :1408.1800v1, August 2014.

[CT06] T. Cover and A. Thomas, Elements of information theory. Wiley-Interscience, Jul. 2006.

[D3.4] SHARING deliverable D3.4, "Flexible interference management concept: innovative concepts and performance evaluation", section 4.1.

[ETW08] R. Etkin, D. Tse, and H. Wang, "Gaussian interference channel capacity to within one bit," IEEE Trans. Inf. Theory, vol. 54, no. 12, pp. 5534–5562, Dec. 2008.

[HAS02] B.Hassibi, B.M.Hochwald, "High-Rate Codes that are linear in Space and Time", IEEE trans. On Info. Theory, Vol 48, No 7, July 2002.

[HEA02] R.Heath, A. Paulraj, "Linear Dispersion Codes for MIMO Systems based on frame theory", IEEE trans. On signal proc., vo 50, no 10, October 2002.

[GHA09] Rizwan Ghaffar, Raymond Knopp, "Spatial Interference Cancellation Algorithm,"*IEEE* Wireless *Communications and Networking Conference*, 2009. WCNC 2009.

[GHA11] Rizwan Ghaffar, Raymond Knopp, "Interference-Aware Receiver Structure for Multi-User MIMO and LTE," 2011/12/1, *EURASIP Journal on Wireless Communications and Networking*, 2011.

[JIN06] N. Jindal "MIMO broadcast channels with finite rate feedback", IEEE Trans. Information Theory, Vol. 52, No. 11, pp. 5045-5059, Nov. 2006.

[KG12] P. de Kerret and D. Gesbert, "Degrees of freedom of the network MIMO channel with distributed CSI," IEEE Trans. Inf.Theory, vol. 58, no. 11, pp. 6806–6824, Nov. 2012.

[KG13] P. de Kerret and D. Gesbert, "CSI sharing strategies for transmitter cooperation in wireless networks," IEEE Wireless Commun. Mag., vol. 20, no. 1, pp. 43–49, Feb. 2013.

[KOT14] S. Kottath, D. Gesbert, H. Khanfir, E. Hardouin, "Broadcast channel feedback in multiple-antenna transmitter cooperation networks: Accuracy or consistency?", EW2014, 20th European Wireless Conference, Barcelona, Spain, May 14-16, 2014.

[KOT15] S. Kottath, D. Gesbert, E. Hardouin, "Opportunistic Feedback Mechanisms in Multicell MIMO Networks," Submitted to IEEE-ICC 2015, London, UK, Jun. 2015.

[MAT12] M. Ali Maddah-Ali and D. Tse, "Completely stale transmitter channel state information is still very useful," *Information Theory, IEEE Transactions on*, vol. 58, no. 7, pp. 4418–4431, 2012.

[MEH09] C. Mehlführer, M. Wrulich, J. C. Ikuno, D. Bosanska and M. Rupp, "Simulating the Long Term Evolution Physical Layer", in Proc. of the 17th European Signal Processing Conference (EUSIPCO 2009), Glasgow, Scotland, Aug. 2009.

[NAG98] A.Naguib, N.Seshadri, A.Calderbank, « Applications of space-time Block Codes and Interference Suppression for High Capacity and High Data Rate Wireles Systems », IEEE 1998.

[NGG09] C. T. K. Ng, D. Gunduz, A. J. Goldsmith, and E. Erkip, “Distortion minimization in Gaussian layered broadcast coding with successive Renement", IEEE Trans. Inf. Theo., vol. 55, no. 11, pp. 5074-5086, 2009.

[RS11] LTE transmission modes and beamforming, White paper, Rhode & Schwartz, October 2011.

[TR25.996] 3GPP TR25.996. 3rd Generation Partnership Project;“Spatial channel model for Multiple Input Multiple Output (MIMO) simulations” (Release 12).

[TR36.814] 3GPP TR 36.814.3rd Generation Partnership Project;“Technical Specification Group Radio Access Network; Evolved Universal Terrestrial Radio Access (E-UTRA); Further advancements for E-UTRA physical layer aspects” (Release 9).

[TR36.819] 3GPP TR 36.819. 3rd Generation Partnership Project; “Technical Specification Group Radio Access Network; Coordinated multi-point operation for LTE physical layer aspects” (Release 11).

[TR36.866] 3GPP TR 36.866 V2.0.0 (2014-02). 3rd Generation Partnership Project; “Technical Specification Group Radio Access Network; Network-Assisted Interference Cancellation and Suppression for LTE” (Release 12).

[TS36.213] 3GPP TS 36.213. 3rd Generation Partnership Project; "Evolved Universal Terrestrial Radio Access (E-UTRA); Physical layer procedures".

[TS136.211] ETSI TS 136 211 V11.2.0 (2013-04), “LTE; Evolved Universal Terrestrial Radio Access (E-UTRA); Physical channels and modulation”.

[YKPS13] S. Yang, M. Kobayashi, P. Piantanida, and S. Shamai, “Secrecy degrees of freedom of MIMO broadcast channels with delayed CSIT,” IEEE Trans. Inf. Theory, vol. 59, no. 9, pp. 5244–5256, Sept. 2013.

[ZG10] R. Zakhour and D. Gesbert, “Team decision for the cooperative MIMO channel with imperfect CSIT sharing,” in Proc. Information Theory and Applications Workshop (ITA), 2010.

GLOSSARY

ACRONYM	DEFINITION
3GPP	Third Generation Partnership Project
AIC	Absolute Interference Cancellation
AWGN	Additive White Gaussian Noise
BC	Broadcast Channel
BER	Bit Error Rate
BS	Base Station
CCUE	CoMP Candidate UE
CoMP	Coordinated Multi-Point
CUE	CoMP UE
CSI	Channel State Information
CSIT	Channel State Information at the Transmitter
DL	Downlink
DoF	Degree of Freedom
eNB	Evolved NodeB
FDD	Frequency Division Duplex
i.i.d.	Independent and indentically distributed
IA	Interference Aware
IA-ML	Interference Aware Max Log MAP
IC	Interference Cancellation
IRC	Interference Rejection Combiner
IS	Interference suppression
LD	Linear Dispersive
LLR	Log Likelihood Ratio
LTE	Long-Term Evolution
MIMO	Multiple Input Multiple Output
MISO	Multiple Input Single Output
ML	Maximum Likelihood

MMSE	Minimum Mean Square Error
MRC	Maximal Ratio Combining
MU-MIMO	Multi-User MIMO
nCUE	No-CoMP UE
JP	Joint Processing
JT	Joint transmission
RAN	Radio Access Network
QoS	Quality of Service
RR	Round Robin
RSRP	Reference Signal Received Power
SAIC	Single Antenna Interference Cancellation
SDoF	Secrecy Degree of Freedom
SIC	Successive Interference Cancellation
SINR	Signal to Interference and Noise Ratio
SNR	Signal to Noise Ratio
SO	Second-Order
SOTA	State of the Art
TDMA	Time Division Multiple Access
TTI	Transmission Time Interval
UE	User Equipment
UL	Uplink
ZF	Zero Forcing